April 2015

Arc-Liberation of Intermolecular Bond Energy for Marine Propulsion

Christopher Michael Byrne
Worcester Polytechnic Institute

Christopher William Egan
Worcester Polytechnic Institute

James Deane Jackman
Worcester Polytechnic Institute

Rohan Jhunjhunwala
Worcester Polytechnic Institute

Tyler Jon Ewing
Worcester Polytechnic Institute

Electrodynamic Water-Arc Propulsion

A Major Qualifying Project

Submitted to the Faculty of

Worcester Polytechnic Institute

in partial fulfillment of the requirements for the

Degree in Bachelors of Science

in

Electrical and Computer Engineering,

Mechanical Engineering,

and Computer Science

By

Chris Byrne

Chris Egan

Tyler Ewing

James Jackman

Rohan Jhunjhunwala

Date: 4/30/15

Sponsoring Organization:

New Energy Foundation

Project Advisors:

Professor William Michalson

Professor Cagdas Onal

Abstract

While modern microelectronics technology has facilitated the development of small, low-power unmanned surface vehicles (USV's), conventional propeller-driven marine propulsion systems are not optimized for such crafts. The proliferation of robotic devices necessitates a novel method of marine propulsion, capable of delivering higher efficiencies than conventional propulsion systems when applied to small-scale watercraft. The goal of the Electrodynamic Water Arc Propulsion (EWAP) project is to develop a solid-state water arc explosion propulsion engine and implement it on a USV. When a high voltage arc is struck through water it has an explosive effect, causing a high pressure pulse, and expelling the water from its holding chamber. In order to apply this phenomenon to marine propulsion, the EWAP team developed several explosion chambers, and evaluated each design through qualitative analysis and subjective observation. The team's research culminated in the development and construction of the final EWAP USV, called the Water-Arc Explosion Vessel – I, or WAEV-I.

Acknowledgements

In addition to our advisors listed above, we would like to thank:

- Jim Dunn, WPI ‘67
- Rober Boisse, WPI ECE shop
- William Appleyard, WPI ECE shop
- Pobco Plastics, Worcester, MA
- Kay Gee Sign and Graphics, Worcester, MA
- The New Energy Foundation and Infinite Energy Magazine

Table of Contents

Table of Figures

1. Introduction

The Electrodynamic Water-Arc Propulsion (EWAP) project began as an exploration of marine propulsion systems alternative to the conventional propeller-driven systems that are commonly used today. The focus was directed towards small-scale marine craft such as single-occupant submersibles as well as Unmanned Surface Vessels (USV's) since these vehicles are only recently becoming commonplace, and propulsion systems have yet to be specifically designed and optimized for them. Since such vehicles often perform life-saving tasks, they require high reliability. As such, a desired characteristic of the propulsion system was solid-state operation, since such a system would not suffer from the wear life of mechanical components.

The initial focus of the EWAP team was to develop a Magnetohydrodynamic Drive (MHD) system that would offer higher efficiencies and thrust forces than those previously developed. Since the majority of the research on MHD was conducted several years ago, this goal was thought to be achievable through the prudent application of modern materials and devices that were not available during previous implementations. Additionally, it was theorized that an MHD system would be well suited to a small-scale craft.

Following the construction and testing of a proof-of-concept MHD thruster, it was determined that MHD requires a higher current or magnetic field than is feasible in order to produce significant thrust force. As such, the EWAP team executed significant literature review in order to discover an alternative to MHD, or to develop a method of increasing MHD performance. During this literature review, the concept of water-arc explosions was discovered, a phenomenon in which electrical energy is used to trigger forceful water explosions. It was thought that water-arc explosion energy could be aptly applied to marine propulsion, providing a forceful solid-state thruster. The team validated the concept of water-arc explosions by reproducing the experimentation performed by previous researchers before developing aseries of "explosion chambers" with the goal of developing an ideal method of applying the phenomenon to marine propulsion. Once significant development had been completed, the team designed a water-arc propulsion system, and installed it on a specially designed USV called the Water-Arc Explosion Vessel-I.

2. Background Information

The EWAP team's original goal had been to develop a method of solid state propulsion and examine its efficiency compared to conventional systems. Prior art in this field had first led the team to pursue magneto-hydrodynamic drive (MHD). However, after designing and building a prototype to validate its functionality, the team decided to explore other methods of solid state propulsion. Electro-dynamic water-arc propulsion had captured the team's interest due to the explosive nature of the phenomenon and potential to provide a suitable thrust for demonstrational purposes. EWAP is a phenomenon which is not well understood or documented, yet prior art and theoretical explanations still exist. The team primarily referred to experiments completed in the past by researcher Dr. Peter Graneau. Graneau had devoted his time to developing water-arc thrusters which provided the team with insight on designing experimental setups both qualitatively and quantitatively.

2.1 MHD Research and Prototype

When an electric current is run perpendicular to a magnetic field in a conductive material, force is created perpendicular three dimensionally to both fields. This relationship between magnetism force and electric current is referred to as Lorentz force. Generally used to describe the force in wire, Lorentz force can also be applied to a conductive liquid such as seawater. In this instance the equation is represented as:

$$F = B \times V \times J \qquad \textit{Eq. 1}$$

Where B represents the magnetic field strength cross product with the volume (V) of the water column and J, the current density vector.[i] The magnetic field is represented by the equation

$$B = \frac{\mu_0 \mu}{\pi} \int_{yo}^{y} x^{-3} dx \qquad \textit{Eq. 2}$$

Where μ_0 is the magnetic permeability of free space and μ is the permeability of the material. The current density vector is represented by the equation

$$J = \frac{\Delta\varphi}{\rho d} \qquad \textit{Eq. 3}$$

Where ρ is the resistivity of seawater, $\Delta\varphi$ is the potential difference between the electrodes, and d is the distance between the electrodes.

2. Background Information

While permanent magnets can be used to create the magnetic field necessary for Lorentz force to operate, the field strength tends to be low and diminishes quickly with distance from the magnets surface. To create a stronger magnetic field electromagnets can be used. These are created by wrapping a wire several times around an iron core supplying it with current. The field created around each wrapping of magnet is transferred to the magnetic core and it circulates all throughout. This interaction is governed by the equation

$$B = \frac{nI\mu}{L} \qquad Eq.\ 4$$

Where *n* is the number of times the wire is wrapped around the core, *I* is the current flowing through the wire, μ is the magnetic permeability of the core and *L* is the length of the core. These magnets have several different orientations that the can be used in since the core can take on many shapes.

To validate the derived physical equations and mathematical concepts, a simplistic prototype was built and tested. Initial calculations were performed to determine a relationship between the device geometry and the theoretical thrust capability. These calculations provided benchmark dimensions, which were helpful in the design process. The design of the prototype was completed via computer modeling, using components sourced from available university resources, as well as online merchants. Following the design phase, the prototype was manufactured using rapid prototyping where possible to facilitate a rapid turnaround time. Testing protocols were developed for the prototype, outlining the testing apparatus, as well as the methods of measurement. Finally, results of the testing were analyzed, and experiment outcomes were discussed in order to determine the prototype's thrust and efficiency.

For this initial prototype, electrical power was to be supplied by an 180W power supply, bridging two 3A channels for a maximum current of 6A at 30V. According to the UK National Physical Laboratory, the resistivity of seawater is 0.200 Ωm at standard ATP, and an average salinity of 35g/kg. Using this value, and the equation $R = \rho\frac{L}{A}$ resistance of the load, and as such the current draw, can be calculated. The length of the tube was chosen to be 4", and the cross-section was to be a 1" square. This allowed us to convert to metric units, this makes L equal to 0.0254m, and A equal to 0.00258m^2. Substituting these values, R is determined to equal 1.97Ω. To ensure the current stays below the 6A capability of the power supply, a potential of 10V was chosen. To solve for $\hat{F}$ in $\hat{F} = \hat{J} \times V \times \hat{B}$, the current density vector $\hat{J}$ must be determined. Using

Equation 4, J is calculated by $\frac{10V}{0.200(0.0254)} = 1968.5\frac{A}{m^2}$. V is trivially calculated by $V = 0.0254m * 0.0254m * 0.1016m = 6.55 \times 10^{-5}m^3$. To find B, properties specific to the magnets purchased needed to be known. The magnetic moment μ_0 was provided by the K&J Magnetics website.[ii] B was found to be 0.7052T, and finally, the thrust force F could be calculated by $F = 1968.5\frac{A}{m^2} \times 6.55 \times 10^{-5}m^3 \times 7.052T = 0.9098N$. Thus, the theoretical thrust output of the prototype engine was 0.9098N.

The design of the prototype was modeled in SolidWorks, using socket cap screws for fastening, PLA plastic for frame elements, and 6061 Aluminum alloy for electrodes. The prototype assembly is shown in Figure 1.

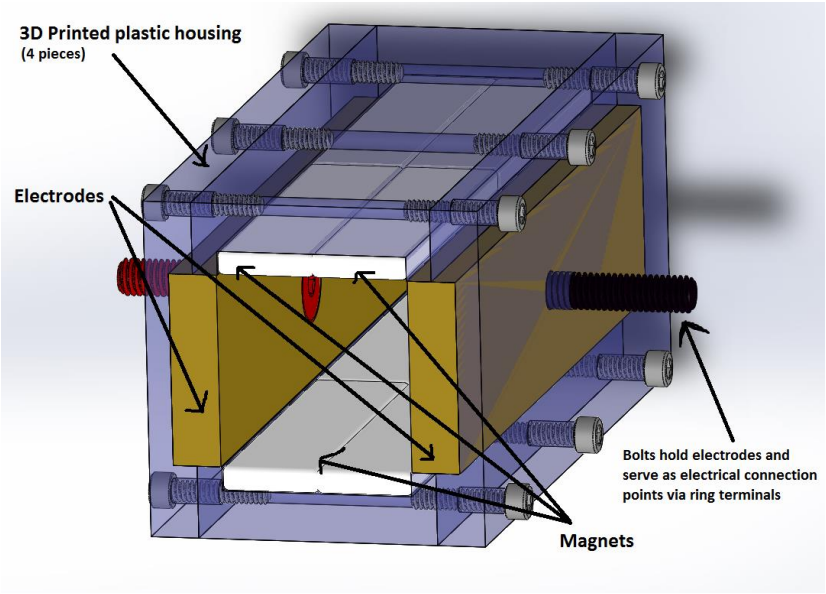

Figure 1: Prototype Thruster Assembly

Grade N42 Neodymium magnets were used to provide a magnetic field, as they are commonly available and provide a relatively high field. The PLA plastic components were manufactured via fused deposition modeling, and the electrodes were CNC machined from aluminum stock. Galvanized steel bolts were countersunk into the electrodes, providing electrical contact points. Once the parts were manufactured, the thruster was assembled, using 6-32 socket cap screws to fix the housing elements, and 2-part epoxy to mount the magnets.

To test the prototype thruster, a salt water bath was made by dissolving 35g of sodium chloride into each liter of deionized water. The thruster was suspended in the bath of water by thin

wires wrapped around the socket cap screws. To view the fluid flow, the thruster was initially oriented horizontally. An image of the apparatus is pictured in Figure 2.

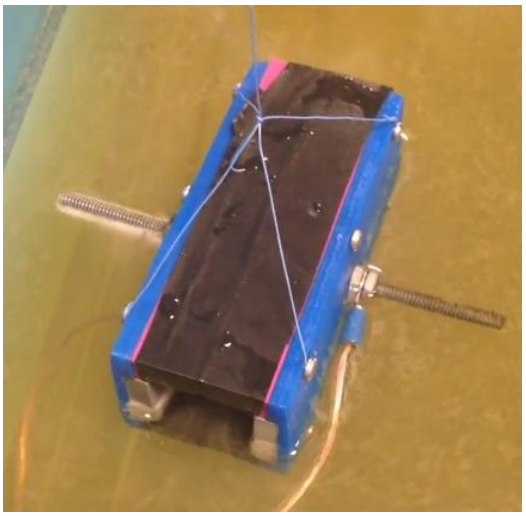

Figure 2: Horizontal Prototype test with Visible Fluid Flow

In the figure above, flow of the water bath can be seen directed down the length of the thruster, indicating functional MHD. The maximum water lift was measured to be 0.375 inches. To determine the thrust force generated by the engine, we used the equation $F = \rho g V$. In our case, ρ is the density of water, equal to 1000kg/m^3, and *h* is the volume of the water lift in cubic meters. The volume V was found to be $V = 0.0254m \times 0.0254m \times 0.0095m = 6.15 \times 10^{-6} m^3$. Substituting these values in the above equation yields $F = 1000 \frac{kg}{m^3} \times \frac{9.81N}{kg} \times 6.15 \times 10^{-6} m^3 = 0.06N$. Though the efficiency of the system cannot be calculated since flow rate was not measured, an estimate of the efficiency can be determined by dividing the measured thrust by the theoretical thrust. This yields a thrust ratio of 6.6%. The thrust ratio indicated that the mathematical and physical concepts behind MHD are limiting. The main hope regarding MHD research was for technology in magnetics to have increased well enough in the past couple of decades to create an efficient MHD vessel cheaply; however, our attention shifted to a less explored method of propulsion, electrodynamic water arc propulsion (EWAP).

2.2 An Exploration of Electrodynamic Explosions

Following the completion of the MHD experiments, the team concluded that the current and magnetic field limitations would prohibit high thrust force and efficiency. During subsequent literature review, several publications concerning a phenomenon known as Water-Arc Explosions

indicated that such a reaction could be applied to marine propulsion. The team investigated the prior art regarding Water-Arc explosions in order to determine the feasibility of applying them to propulsion. When a large amount of voltage is discharged through water it has an explosive effect, causing the water to be expelled from its holding container. Minimal energy appears to be lost from this reaction, as no significant change in water temperature is observed. Furthermore the explosion can be very loud. Although this form of reaction has been known for quite some time the underlying reason for its occurrence remains unclear.

While the cause is still unknown several ideas have been proposed to explain this phenomenon. The initial thought was that the reaction was caused by superheating and rapid expansion of water. While this seems like an obvious solution, no steam or large change in water temperature has been detected during the reaction, making this cause unlikely. A fog of small groups of water molecules visible following a reaction have also been used to explain its cause. It was hypothesized that these smaller droplets have a smaller bonding energy than liquid water, so when the liquid was converted this excess of bonding energy was released resulting in an explosion.

To verify this hypothesis and to rule out the possibility that hydrogen and oxygen gas rapidly created from electrolysis was creating the explosion, the team performed the following calculations based on the maximum energy storage capacity of a 4µF capacitor charged to 12kV. First, the team calculated the volume of hydrogen and oxygen gas that could theoretically be created with the assumption that there were no other energy loses. These calculations can be seen below.

$$2H_2O \xrightarrow{237.13kJ/mol} 2H_2 + O_2$$

$$Max\ Capacitor\ Energy = 0.5 * 0.000004 * 12000^2 = 288J$$

$$Explosion\ Chamber\ Volume = (\pi * 0.333^2) * 3.93 = 1.367in^3\ or\ 0.0224L$$

Hydrogen Gas:

$$\frac{237.13\ {}^{kJ}/_{mol}}{288\ J} * \frac{2\ mol\ H_2}{3\ mol\ products} * \frac{2.02\ {}^{g}/_{mol}}{1} * \frac{1}{0.0899\ {}^{g}/_{L}} = 0.0178L\ of\ H_2$$ [iii]

Oxygen Gas:

$$\frac{237.13\ {}^{kJ}/_{mol}}{288\ J} * \frac{1\ mol\ H_2}{3\ mol\ products} * \frac{16\ {}^{g}/_{mol}}{1} * \frac{1}{1.4290\ {}^{g}/_{L}} = 0.0045L\ of\ O_2$$ [iv]

From these calculations of the volume of hydrogen and oxygen gas created from electrolysis, there would be 0.0223L of gas that would be expelled from the explosion chamber during a water arc explosion. These would mean that the amount of gas created during an explosion chamber would be the same as the volume of the chamber itself. However, during the testing discussed later in this paper, the team did not observe any gas bubbles large enough to hold a volume of gas comparable to the volume of the explosion chamber.

Previous tests have shown that it generally takes anywhere between 6-10kV for an explosion to occur. The voltage required for an arc to strike is affected by the distance between the electrodes. The discharge time only lasts for a few microseconds, during which peak current can exceed over 100A. Figure 2 depicts a testing apparatus used by Graneau during one of his force measuring experiments. Force measurements were taken by suspending a 2.8g weight on the surface of the water. The weight was launched a height of 20cm resulting in a force of 21.6N.[v]

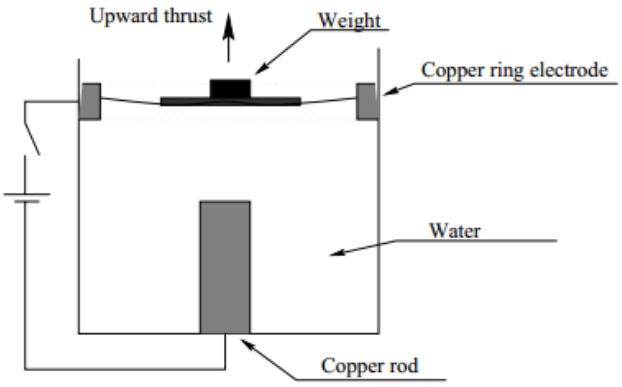

Figure 3: Testing Apparatus

Based on experimental results it has been theorized that this phenomenon could be used as a method of propulsion. One of the proposed jet designs as shown in Figure 4, intakes water from one side and expels it from the other creating forward momentum. The force of this jet can be approximated using the equation:

$$F = \frac{\mu_0}{4\pi} k I^2 \qquad \textit{Eq. 2}$$

where μ_0 is the magnetic permeability of free space, I is current, and k is a geometrical constant determined by the shape of the jet.

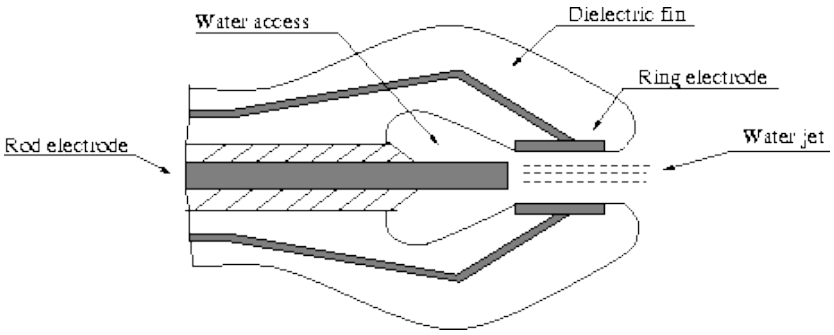

Figure 4: Electrodynamic Explosion Jet Design

The majority of the existing research on the water-explosion phenomenon describes the use of several-kilovolt pulses of electricity discharged through a capacitor, delivering over half a megawatt of power in some cases. As such, great care was taken in the high-voltage circuit design to prevent failure of components, and safety precautions have to be outlined prior to any experimentation. All experiment designs, procedures, and safety protocols were thoroughly vetted by advisors and laboratory personnel before any lab work. To expedite this process, the team has developed a design for a high voltage circuit, and outlined basic safety procedures for testing, presented in the following sections.

2.3 Early Experimental Test Circuit

In order to successfully create an explosive water arc a custom circuit must be designed that is capable of discharging a large amount of voltage and current through the water or load. This circuit will have to be able to create the high voltages needed to charge the capacitor and then quickly discharge the capacitor once it is fully charged. An example of what such a circuit could look like can be seen below in Figure 5.

2. Background Information

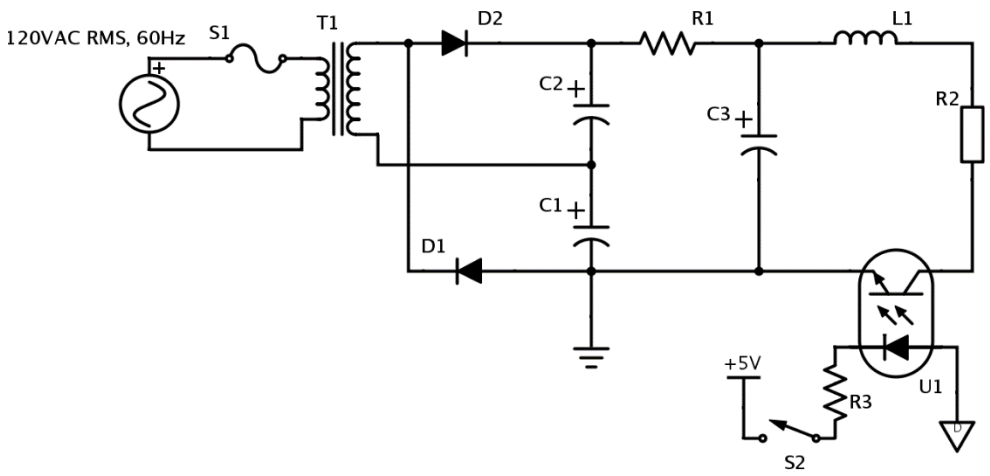

Figure 5: Theoretical Circuit design

In the example circuit a standard 120V AC power is fed through a protection fuse to the primary windings of T1. T1 is a HV magnetron transformer with approximately 60 windings in the primary and 1000 windings in the secondary to step the 120VRMS up to 2kVRMS. D1 and D2 rectify the 2kVAC, charging C1 and C2 to about 2.8kVDC each. This voltage is applied in series to charge a high capacity capacitor C3 through R1, to about 5.8kVDC. C3 must be rated above 5.8kV and must have a capacitance of around 1µF. Once the capacitor is charged, the optoisolator U1 transistor output is closed by activating the internal LED, which can be achieved as in the example by a simple switch S2, or by low voltage control circuitry. By using an optoisolator, the low voltage circuitry is isolated from the damaging high voltage generator, enabling safer operation. Once the isolator is triggered the capacitor C3 discharges through an inductor L1, increasing the current which is then applied to the seawater load R2. This should elicit an explosive reaction to occur in the seawater causing it to be ejected from its container.

C3 is charged to 6kV as used in previous experiments. In the example circuit, D1, D2, C1, and C2 form a half wave rectifier voltage doubler. In the future, this circuit topology can be repeated, forming a Villard cascade, allowing higher voltages to be achieved. A single high voltage high capacitance capacitor could be used for this purpose, however, if higher voltages are required, several capacitors could be connected in series. With 1 µF total capacitance at 5.8kV, the equation $q = CV$ dictates that the capacitor will hold a charge $q = 1\mu F(5.8kV) = 5800\mu C$. Over a pulse of t =50µs, this will allow a current of $I = \frac{q}{t} = \frac{5800\mu C}{50\mu S} = 116A$. The power delivered to the water at this current would be $116A(5.8kV) = 673kW$. These quantities are consistent with those that

elicit a water-arc explosion, according to a 1992 subject on water explosions by Dr. Gary Johnson of Kansas State University.[vi]

3. Obtaining Water-Arc Explosions

In order to generate a water arc explosion, a high voltage circuit needed to be designed and built. This circuit would have multiple stages to charge and rapidly discharge a large capacitor through a column of water. A high voltage power supply would have to be built, capable of generating around fifteen thousand volts. An RC charging circuit would have to be designed, containing a high voltage capacitor, and an appropriate charging resistance. To discharge the capacitor an appropriate discharge circuit was needed that could be controlled remotely and handle multiple high energy discharges from the capacitor without breaking down. Finally the explosion chambers need to be designed that could discharge the capacitor's energy through a column of water, and direct the explosive reaction without breaking. As the first component of the circuit, the high voltage power supply was looked at first.

3.1 High Voltage Power Supply Design

When creating the high voltage power supply multiple design specifications were considered. The power supply would have to be able to generate around fifteen thousand volts, produce a sufficiently high current, and be an appropriate size and weight. A couple design options were found that could fulfill these requirements, ranging from pre-built systems to general circuit concepts. To quantitatively analyze these power supplies, a high voltage probe was used to analyze the output waveforms produced. The first potential power supply that was examined in depth was the flyback transformer.

3. Obtaining Water-Arc Explosions

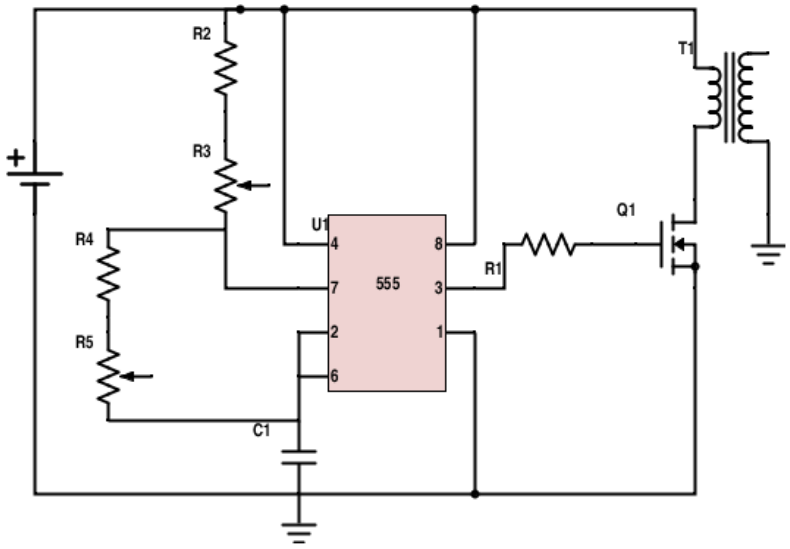

Figure 6: Flyback Transformer Circuit with 555 Driver Circuit

Flyback transformers are used in CRT TVs to generate high voltages at high frequencies. This transformer operates by supplying a pulsed low voltage waveform to an inductor, causing the inductor to build up a magnetic field flux when the pulse is high. When the input voltage is low the magnetic field declines rapidly and induces a voltage much higher than the input voltage. This design allows for high voltages to be generated from low voltages without the need for large turn ratios, greatly reducing weight. While it would be advantageous to have a lightweight power supply, the flyback transformer was unable to produce a current capable of charge the capacitors quickly and its output voltage waveform was inconsistent. Keeping these drawbacks in mind, other supply designs were considered.

A dc-dc boost converter generates high voltages from low voltages by using a similar principle to the flyback transformer. A low voltage is applied to an inductor through a switch, and when the switch is closed, flux builds up in the inductor. When the switch is open the flux collapses generating a high voltage which is used to charge a capacitor through a diode. In practical applications, the switch is rapidly pulsed on and off. The capacitor can then be used to discharge high voltages over a resistive load. Like the flyback transformer this design is small and compact but also reduces the output current, limiting the charge time. Furthermore the capacitor required for this circuit would have to be at least as big as the charging capacitor, and the duty cycle of the switch would have to be incredibly fast. For these reasons this design was impractical for generating large voltages.

3. Obtaining Water-Arc Explosions

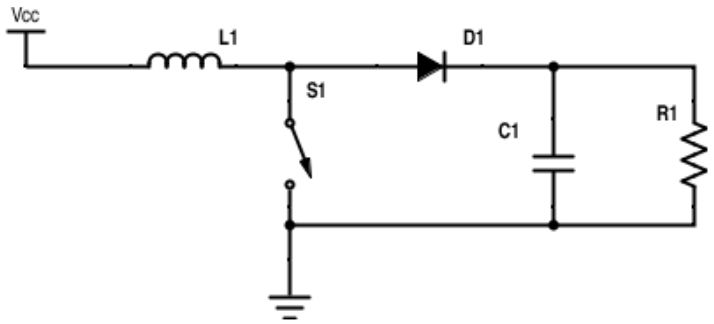

Figure 7: Basic DC-DC Boost Circuit

A Cockcroft-Walton generator or voltage multiplier uses a cascade of diodes and capacitors to create high output voltages form an AC voltage source. A basic doubler contains four diodes and four capacitors. When the input AC voltage is negative the first capacitor is charged through the first diode to the max input positive voltage. When the waveform peaks positive the voltage on the capacitor adds with the supply voltage and charges the second capacitor through the second diode to twice the maximum voltage. This process is repeated with the remaining diodes and capacitors to achieve a DC voltage that is double the peak input voltage. It can take multiple cycles for the final capacitor to charge up to its maximum value, and additional stages can be added triple or quadruple the voltage. While this circuit could be used to generate high voltages the amount of stages it could take to do so may make its use impractical, as the charging time would increase for every stage. However it may be useful if used in conjunction with another power source like the boost converter.

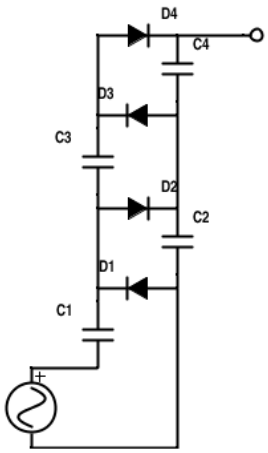

Figure 8: Voltage Multiplier

While looking at pre-built transformer designs, a neon sigh transformer was brought up for consideration. Generally used to excite gasses in neon tubes to make light, the NST was capable

of producing 12kV RMS consistently, and delivering up to 30mA. The main drawbacks of this transformer were its size and considerable weight. The NST weighed in at around 30lbs due to its internal asphalt insulation. However considering its ability to produce the desired output the neon sign transformer was selected for preliminary water arc testing.

Since the DC voltage was needed to charge the capacitor, the output waveform of the NST needed to be rectified. A half wave rectifier was created using high voltage diodes found on campus. These diodes could individually handle 15 kV each so they were used in series so they could safely handle more voltage. Two high voltage terminals were found locally and were used to create the power supply output terminals.

3.2 High Voltage Capacitor Selection

The capacitor chosen for the charging and discharging circuit had to be capable of charging to at least ten thousand volts and have a capacity of at least one microfarad. These types of capacitors proved difficult to find as their application range is fairly narrow. Avenues for purchasing a capacitor, such as local, online and second hand sources were explored. Although an appropriate capacitor could not be found locally a capacitor was eventually found online, from a seller in China. This film capacitor could charge up to fifteen thousand volts at two microfarads and was relatively lightweight. While this capacitor was ideal for the charging circuit, since the seller was located outside the country the shipping time problematic. This capacitor was purchased for the final design, however since testing needed to begin, temporary options for capacitors were explored.

Many high voltage capacitors are used for power line transmissions. By searching within this application set, a couple of second-hand power film capacitors were found. Two of these capacitors were purchased, one rated for ten thousand volts at one microfarad and the other fifteen thousand volts at one microfarad. These capacitors were large, bulky and contained the dangerous chemical PCB, which is an environmental and health hazard. Considering the potential hazard and the age of the capacitors, great care was taken to condition these capacitors to operate at high voltages.

A high charging resistance was used to ensure that the capacitors were not charging too rapidly. Seven 6.3 mega ohm resistors were used in series for a total resistance of 44.1 mega ohms.

Using the capacitor charging equation shown below the charging time was found to be 58.9 seconds when charging to 12 kV.

$$V_C(t) = V_F(1 - e^{\frac{-t}{RC}})$$

Since the power supply was only half wave rectified the actual charging time would be longer than this calculated value, however it for early testing purposes this was acceptable.

3.3 Discharge Circuit Design and Construction

The discharge circuit, responsible for dumping all the energy stored in the capacitor into the explosion chamber, had to be able to withstand both high voltage and high current without breaking internally. A switch is connected to the capacitor that, when closed, rapidly discharges the capacitor. The first attempt at creating this circuit involved using a high voltage relay to control the discharge of the capacitor. Using a relay would provide a large amount of control over the capacitor discharging, which would be useful for implementing control systems. A relay, rated at 10kV, was initially used to fulfill this purpose to little success. The relay succeeded in discharging the capacitor twice before the internal contacts welded together resulting in a permanent short circuit. A 15kV gigavac vacuum tube relay was purchased in the hopes that it could handle the initial current spike from the capacitor, however after its second use it also failed. It became clear, that an alternative discharging switch was needed.

As the impedance in the capacitor discharge is quite low, the current delivered by the capacitor during the short discharge pulse can be very high. Some researchers have reported currents in excess of 1kA with similar experimental setups. This is very demanding on the contacts of the relay, even vacuum chamber relays designed for high voltage discharge applications are rarely rated for currents in excess of 50A at 10kV. To allow the water explosion to be electronically triggered, a custom high voltage switch was designed, actuated pneumatically and controlled by a solenoid valve.

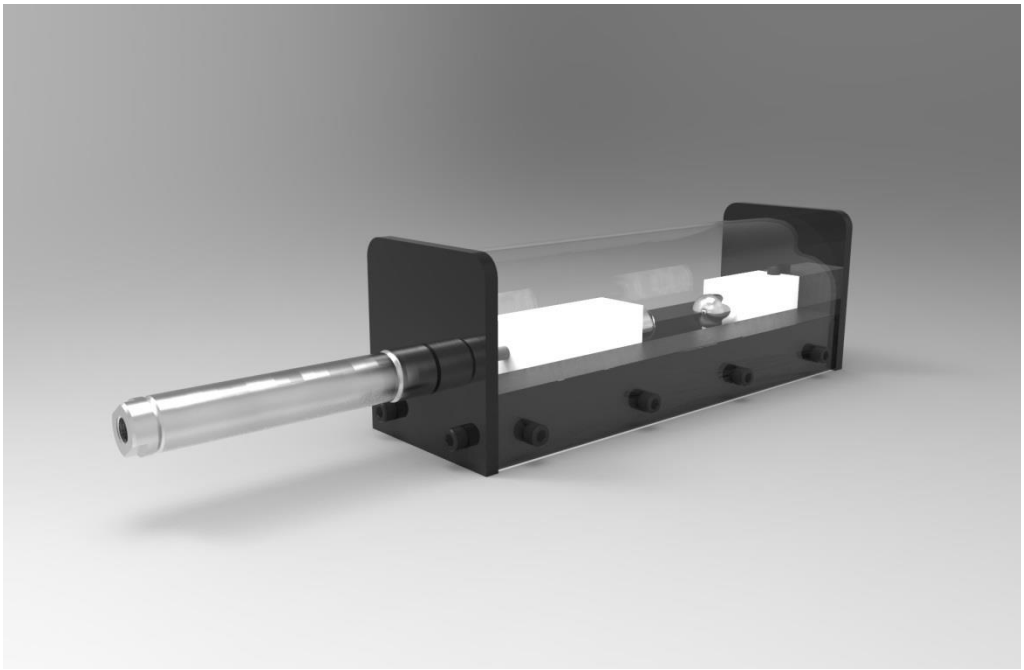

Figure 9: Pneumatic Switch

Two hemispherical steel electrodes are mounted to UHMW insulators inserted into a low-friction PVC track. One insulator is fixed to the track, while the other is mounted to a pneumatic cylinder and allowed to slide axially. This cylinder could be controlled when provided with a 12 volt signal. When the cylinder extends, the two electrodes are brought within a millimeter from each other, and the small air gap is easily ionized to form a low impedance bridge. The electrodes are kept from touching in order to prevent them from fusing together.

3.4 Explosion Chamber Considerations

The first explosion chamber was designed to minimize the possibility of catastrophic failure under the explosion forces. Stainless steel rods were machined with three different bore diameters, seen in the figure below, and inserted into a shock-absorbing wooden block. Acetal Copolymer plugs were press-fit into the end of the stainless steel barrels, and a 6-32 tapped hole was machined into them to accept the ground electrodes. Finally, three 8-32 tapped holes were machined into the stainless steel explosion chambers, to provide electrical connection points.

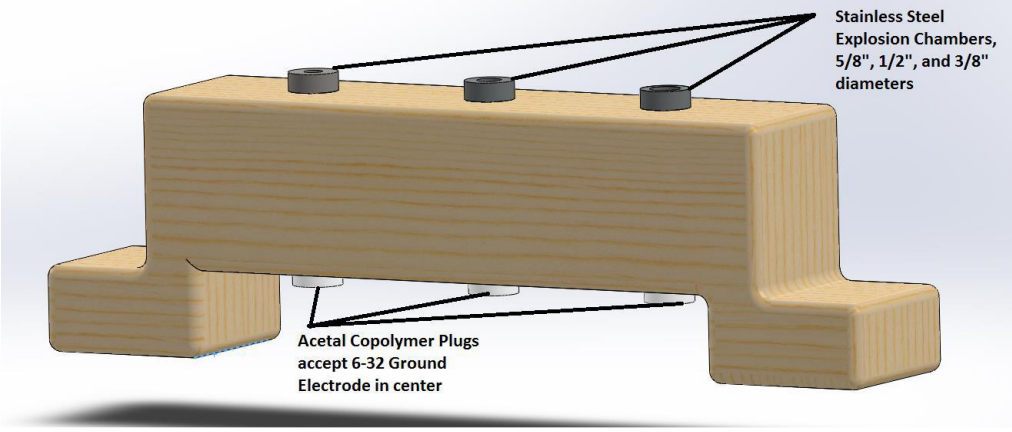

Figure 10: Explosion Chambers and Containment Block (Chamber I)

The bore diameters of the chambers were selected based on previous experiments performed on water-arc explosions. The intent of having different hole diameters was to allow for testing of water-arc explosions under different conditions to see which produced the most powerful explosion.

3.5 Experimental Method

After all components of the circuit were assembled the initial testing of the system began. Initial water-arc explosion experiments were conducted in order to determine the necessary parameters to achieve reliable water-arcs. A high voltage probe was used to monitor the voltage on the capacitor. Once a voltage of 6kV was achieved, the transformer was shut off and the circuit was discharged through the pneumatic switch. As the capacitor was discharged though the explosion chamber the 2ml of water in the chamber was propelled upwards at high speeds. Knowing that the circuit was cable of generating the desired explosions, the force of the reaction had to be quantified.

To test the explosion force generated, a UHMW projectile, weighing 34g, was placed on top of an explosion chamber filled with 2ml of water. During the explosion event, the projectile was lifted upwards, as water was rapidly propelled from the chamber. A ruler placed behind the chamber allowed for the projectile's maximum height to be recorded by a high frame-rate camera. Once determining the maximum height reached by the projectile, the energy transferred to the projectile from the explosion could be determined.

In addition to quantifying the force of the reaction, other tests were performed in an attempt to gain a greater understanding of water arc explosions. Arcs were fired at a wide range of voltages to determine the lowest voltage an arc could be fired at, and to see how the explosive force is stronger at higher voltages. Images of the resulting water fog jets were analyzed to see what form the water takes when after the reaction has occurred.

3.6 Testing and Results

There were two main objectives in this round of testing. The first was to determine the lowest possible voltage water arcs could be fired at. When charged to 5.75kV the resulting explosion using 2ml of water barely managed to lift the 34g cylindrical projectile therefor 5.75kV was determined to be the lowest voltage that could create water-arcs. The next variable quantified was the energy used to move the projectile. Still only filling the chamber with 2mL of water, the voltage was raised in 0.5-1kV increments until the projectile was able to reach its peak height at the top of where the ruler was positioned. At a 9kV charge the projectile reached a height of 17.5in. This projectile at its maximum height can be seen in the figure on the following page.

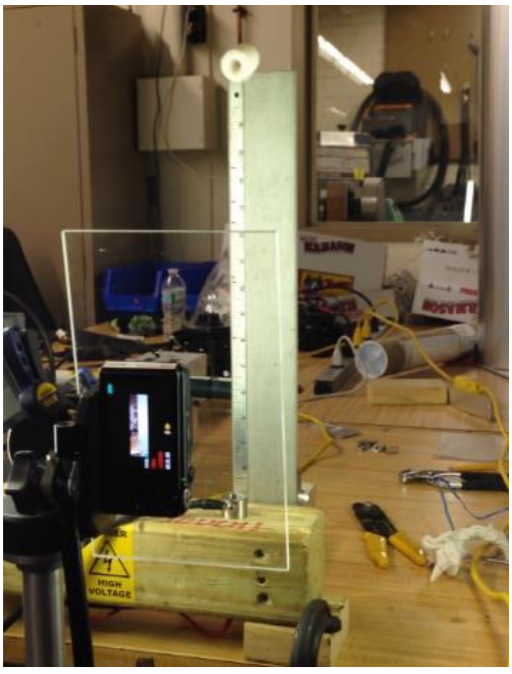

Figure 11: Projectile Maximum Height

The total energy stored in the capacitor is given by the equation $E_c = \frac{1}{2}CV^2$. The capacitor is rated to 1uF. Since there was 1 kV remaining on the capacitor after the arc has fired, a value of

8 kV was used. Using these numbers the energy output of the capacitor was evaluated to be 32J. The potential energy of the projectile is given by the equation $PE=mgh$. Where m, the mass of the projectile, is .034kg, g is 9.8 m/s^2, and h is the maximum height, 44.45cm. The maximum PE of the projectile was calculated to be 0.148 J. Therefor efficiency of launching this projectile is 0.4%. However this does not take into account energy losses within the system including the chamber design itself and the transfer of force between the water and the projectile. During the final water-arc explosion the Acetal Copolymer plug of the chamber was dislodged from the stainless steel cylinder. With this in mind it was necessary to design a new chamber that would not contribute as greatly to the system losses.

4. Quantifying Water Explosions

Once it was demonstrated that water-arc explosions could be reliably produced, the team began to focus on quantifying the fluid parameters, forces, and energy produced by the explosions. In order to do this, the team produced chamber design revisions, and conducted several experiments in order to quantify the explosions produced in the chamber. The team focused on apparatus development, instrumentation, and experimental design to obtain water-arc explosion measurements that will influence the design of the water-arc thruster.

4.1 Desired Performance Metrics

After successfully obtaining water-arc explosions, it was necessary to develop a quantitative understanding of the phenomenon in order to apply it to marine propulsion. Before setting out to develop experimental procedures to measure water-arc explosions, two parameters, or performance metrics, were identified as being the most useful to measure. The first performance metric was arc duration. By determining the duration of the explosion event, it was possible to calculate the current delivered by the energy storage capacitors. This not only influences circuit design, but also allows us to calculate the power delivered to the explosion chamber. In addition to arc duration, the energy output of the explosion is a useful performance metric, as it provides a comparison to the input electrical energy. While energy output is difficult to measure directly, several indirect methods of measurement were considered before the experiment was conducted.

4.2 Chamber Revisions

The second chamber was crafted from a solid two inch rod of Ultra-high-molecular-weight polyethylene. UHMW not only has the among highest impact strength of all thermoplastics, but also has a very high dielectric constant, making it ideal for these high voltage, high stress applications. The rod was cut into a five inch segment and a 5/8 inch hole was drilled four inches deep. Two small holes were drilled and tapped into opposite sides of the chamber towards the bottom of the drilled hole. These holes were outfitted with two plugs containing two brass electrodes. The plugs were designed to leave room for wire connections to the electrodes, while also securing the electrodes tightly in the chamber. To prevent the plugs from moving in reaction to the forces being generated, adhesive was used to fix them and the electrodes in place. In the back of the explosion chamber, a ¼-20 tapped hole was added to act as mounting point. The

resulting chamber was mounted to a wooden table top so the force would be projected upwards and there would be little chance of it shifting positions. A cad drawing of this chamber can be seen below.

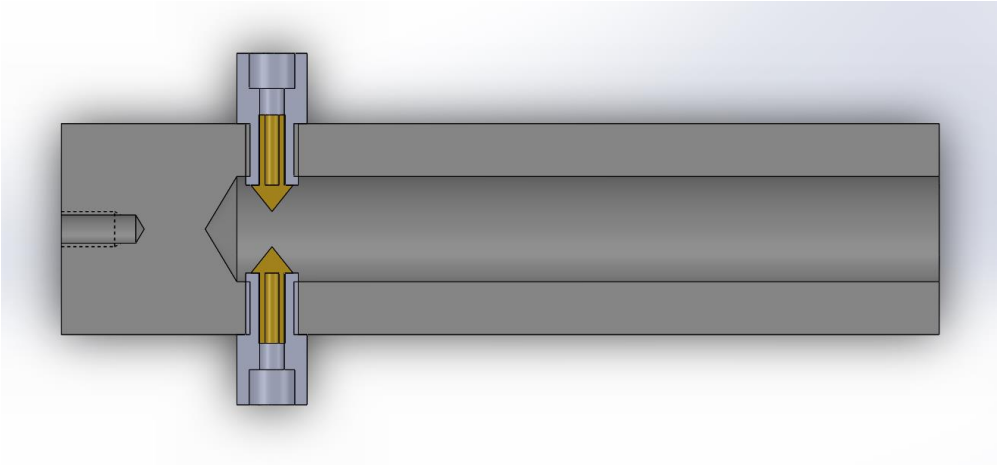

Figure 12: Cross-section of Mark II Explosion Chamber

As can be seen in the cross sectional image above, water is only has one way in and out of the chamber. This directs the force of the reaction in one direction maximizing the force output. In an underwater environment the water expelled out would have to flow back in before another arc could be fired. While simple, this aspect of the design could affect its performance as a propulsion unit.

4.3 Arc Duration Experiments

To determine the average current of an arc discharge event, several measurement methods were developed. Since the average current is equal to $\Delta q \Delta t$, and we know that the charge delivered by the capacitor is $q=C(Vi-Vf)$, we can determine the current by measuring the time of capacitor discharge. To measure this time, it was initially thought that the capacitor voltage oscillogram during a discharge event could be used to determine the duration of the discharge. The following figure depicts the oscillogram of a 12kV discharge.

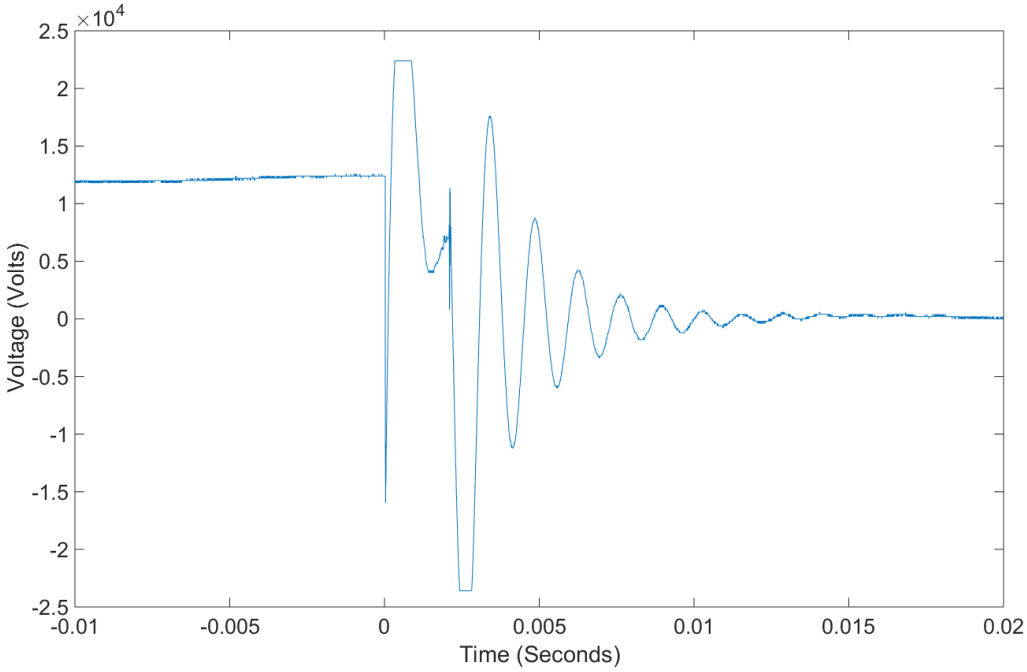

Figure 13: Capacitor Discharge Waveform

While the waveform appears to exhibit the standard damped sinusoidal decaying waveform for capacitor discharge, it is difficult to estimate the arc duration from the plot. We can assume, however, that the erratic nature of the waveform in the 0-2.5ms range indicates an unstable impedance – which would be characteristic of the impedance of an arc. As such we can use this method to estimate an arc duration of 2.5ms.

An arc duration of 2.5 milliseconds seems quite long compared to the results presented by previous researchers, so a second method of arc duration measurement was devised in order to confirm the previous results. This method utilizes a photodiode to produce output proportional to the brightness of the explosion chamber. During an explosion event, the arc illuminates the chamber and surrounding area, which can be easily detected by the photodiode. The photodiode current was amplified by a transimpedance amplifier, and the output was viewed on an oscilloscope in order to measure time. The resulting oscillogram is depicted below.

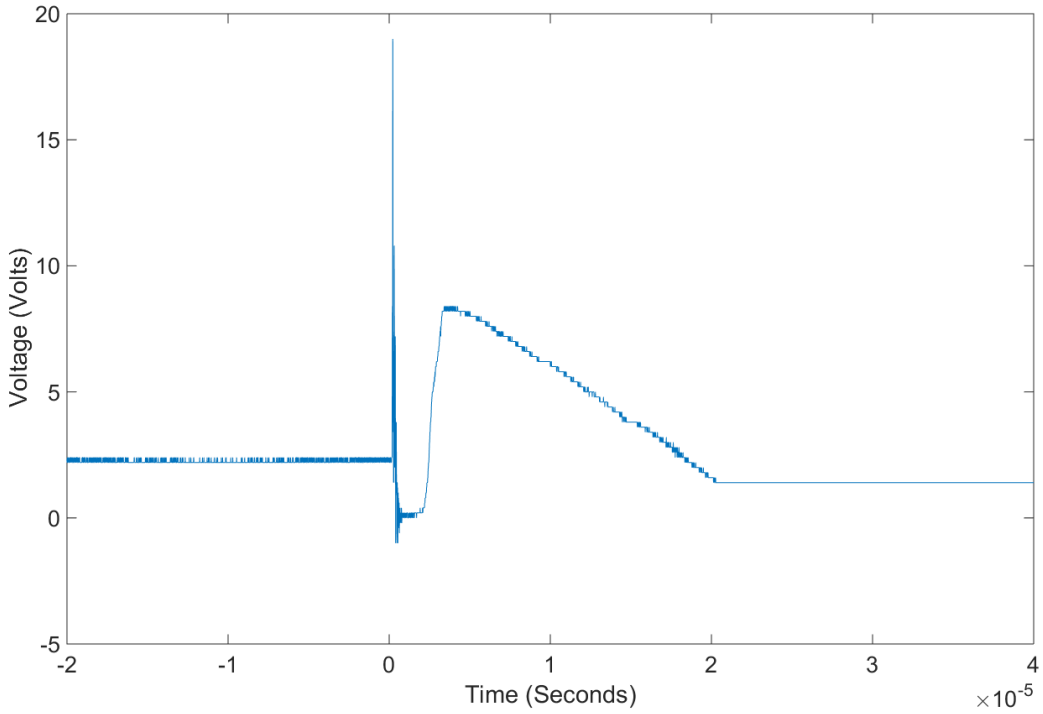

Figure 14: Photocell oscillogram

The initial high voltage peak was determined to be due to electromagnetic inductance from the discharge event. Thus, we can assume that the arc began at the instant this peak occurs. The LM741 Op-Amp IC that was used to build the transimpedance amplifier for the photodiode contains overload protection circuitry, which was likely activated due to the EM inductance. Thus, the output of the amplifier drops to zero just after the protection circuitry is activated, which can be seen on the oscillogram from about 1-2.5 microseconds. Following this, the amplifier resumes normal operation in time to show the remainder of the arc flash. Before t=0, the amplifier's output is due to the ambient light in the room which is incident upon the sensor's active area. During the arc flash (visible after t=3µs), the output of the amplifier climbs much higher than the ambient light value, and falls back down as the arc flash dies out. Thus, we can determine the arc duration to be the time from the initial peak until the voltage settles again, or about 21µs.

For this test, the 2µF capacitor was charged to 12kV, and had a residual voltage of 131V after the arc. Thus we can calculate the current:

$$I = \frac{2\mu F(12kV - 131V)}{21\mu s} = 11.3kA$$

The value of 11.3kA, while quite high, is similar to the currents reported by other researchers.

4.4 Time of Flight Testing

In addition arc duration testing, the version 2 explosion chamber was used to perform experiments to measure the energy output of the explosion machine. Because the explosion event happens in such a short amount of time, the explosive pressures and forces cannot be measured by conventional load cells and resistive pressure sensors. As such, an experiment was devised involving transferring the explosion energy to a projectile of known mass.

The projectile that was used was an aluminum plate with a mass of 94.3g. The plate was positioned on top of the explosion chamber, which was oriented vertically upward. The explosion chamber was wrapped with a steel hose clamp which was flush with the top of the chamber, such that the aluminum plate made contact with the hose clam when positioned on top of the chamber. A 10V potential was applied to the hose clamp, and the aluminum plate was connected to an oscilloscope. The oscillogram pictured below is the result of a 11kV arc fired with 5mL of water in the chamber.

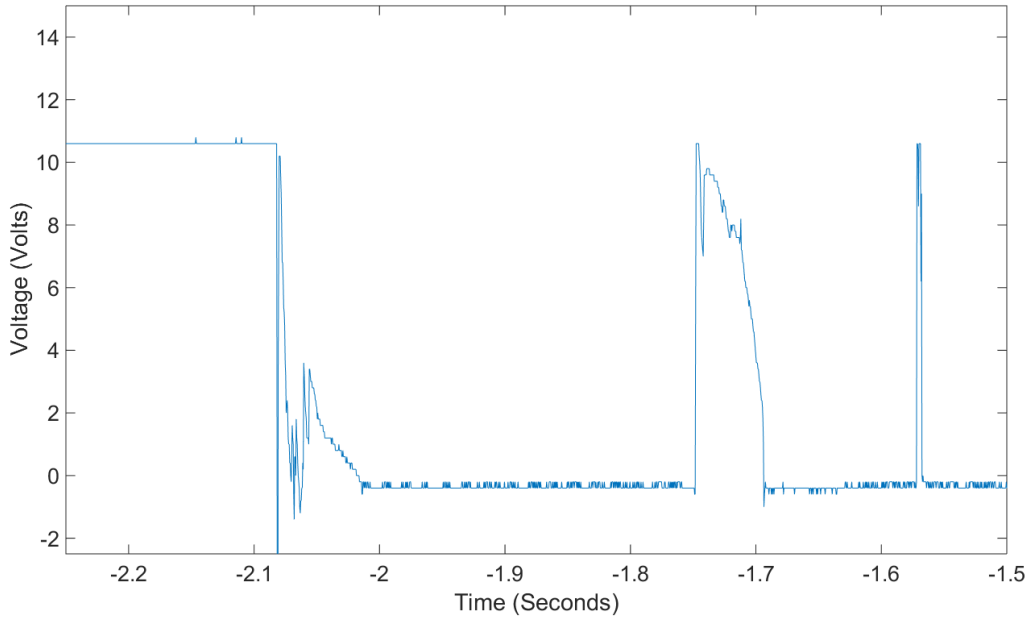

Figure 15: Time of Flight Testing Oscillogram

Before the explosion, the 10V potential is conducted between the hose clamp and the aluminum plate, which can be seen on the oscilloscope. When the explosion is triggered, the explosive force from the chamber lifts the plate, breaking electrical contact, causing the oscillogram to return to 0V potential. After attaining a maximum height dictated by the amount of energy transferred from the explosion, the projectile falls back down to once again make contact with the hose clamp, and the oscillogram returns to 10V. Because the force of gravity is the only force acting upon the projectile during flight, we can estimate its maximum height using the time of flight, which is equal to the time for which the voltage is 0V in the above plot, or 334ms. Since the projectile attains its maximum height in half the total time of flight, we divide this value by 2 to yield 167ms. Using kinematics, we can find the maximum height:

$$h = \frac{1}{2}gt^2 = \frac{1}{2}(9.81)(0.167)^2 = 13.7cm$$

Thus, we can determine the energy of the 94.3g projectile at this height:

$$E = mgh = 0.0943 * 9.81 * 0.137 = 0.127J$$

While this value seems quite low, there are several loss mechanisms associated with using this method of energy measurement. Namely, the fraction of the explosion energy which is transferred to the projectile is likely quite small, especially since the water from the explosion is almost completely evacuated from the chamber, and droplets were found quite far from the explosion area.

4.5 Thrust Force

As a rough approximation of thrust force, a final test was performed. A wooden platform was placed on top of the chamber, and a 1-liter plastic bottle was filled half-way with water. When the explosion occurred, the platform was fired upwards and did not remain on top of the chamber. The water in the bottle was increased in 100ml increments until the explosive force was equal to the weight of the platform, bottle, and water, such that the explosion did not cause the platform to move. The weight of the water, bottle, and platform was 1.1kg, indicating a potential thrust force of 10N.

4.6 Discussion

The experimentation described above was performed in order to influence the design of future explosion chambers, with the goal of optimization for underwater propulsion. The results

from the Time-of-Flight testing as well as the current measurements indicate that there is a substantial amount of power input to the explosion chamber, and much of that power can be seen in explosive force. This suggests that the water-arc phenomenon lends itself well to jet propulsion. Furthermore, the estimated thrust force of 10N is likely to be sufficient to propel a demonstration USV to showcase water-arc propulsion.

5. Developing a Water-Arc Thruster

5.1 Testing Apparatus

With the experience and data obtained during prior experimentation, the next phase of development focused on creating submerged water-arc explosion chambers, and evaluating their performance in order to determine the optimal jet thruster design. To test the iterations of explosion chamber designs, an underwater testing apparatus was constructed to measure their thrust force. A diagram of the assembly is shown in the figure below.

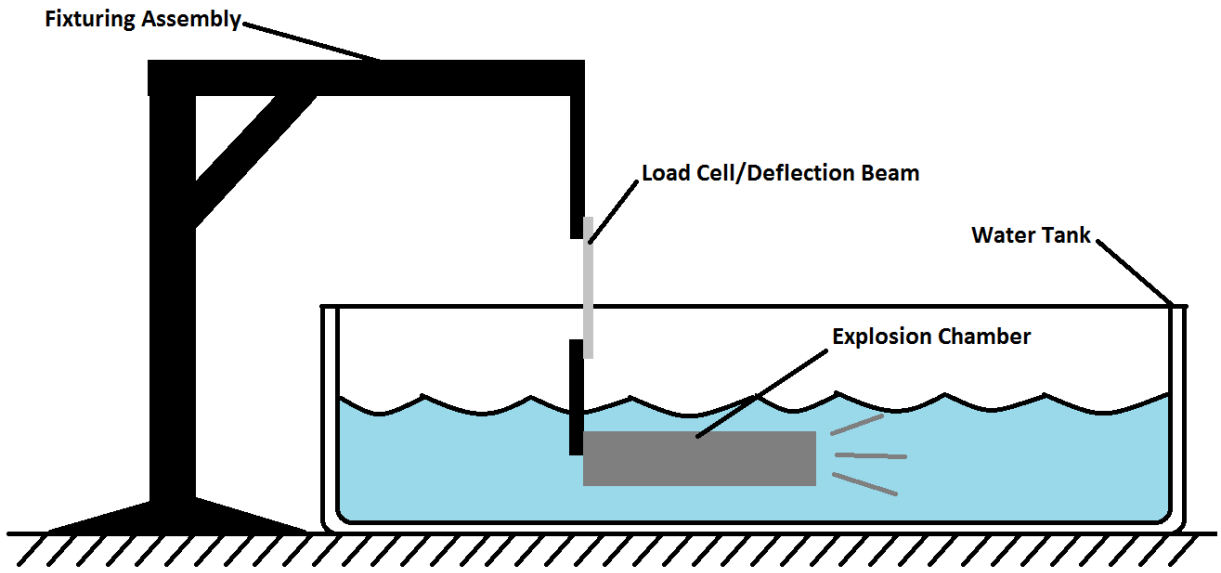

Figure 16: Underwater Testing Apparatus

Initially, a 20kg load cell was purchased, and installed as indicated in the above diagram. An instrumentation amplifier was used to amplify the load cell signal, and the resulting signal was displayed on an oscilloscope. Initial test arcs showed severe electromagnetic interference from the capacitor discharge event, making the load signal illegible. Fortunately, this issue was solved simply by moving the oscilloscope and electronics far from the explosion site. However, once the sensing circuitry was sufficiently isolated, the load cell oscillogram appeared as a relatively flat line, despite the large forces imposed by the explosion. This was thought to be due to the short duration of the thrust impulse, which occurred faster than the response time of the electronics. As such, subsequent thrust calculations were performed by completing a stress analysis of the beam deflection of the fixturing assembly.

5.2 Explosion Chamber Mark III

5.2.1 Design

The third explosion chamber, influenced by Dr. Graneau's theoretical jet design, was created with the goal of obtaining a continuous water jet. By having continuous water flow, the chamber would be optimized for boat propulsion. This chamber was made out of the same material and had similar dimensions as chamber version II. A copper tube was used to line the explosion chamber acting as an electrode. The other electrode, a brass rod, was centered in the back of the explosion chamber. The main difference between this explosion chamber and the previous revisions are the inlet holes located in the back of the chamber. A CAD drawing of this design can be seen in Figure 17 below.

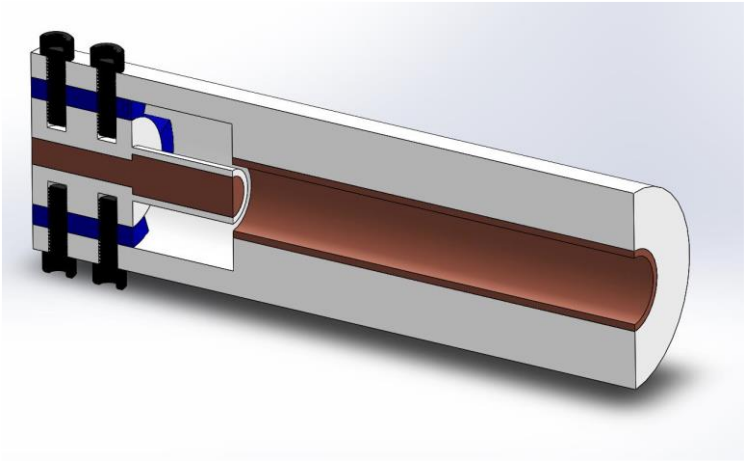

Figure 17: Cross Section of Mark III Explosion Chamber/Jet Design

As can be seen in Figure 17, the main structure of the explosion chamber is made of the same UHMW plastic for its high tensile strength. The explosion chamber is lined with a 5/8 inch diameter copper pipe as one of the electrodes. The second electrode is centered in the back of the chamber, secured in place by another UHMW part allowing it to withstand any blowback forces due to the water explosion. To center and secure this piece, a series of screws are aligned on the outer enclosure and are screwed into the centering part. These screws keep the part from being forced out the back during an explosion and allow for quick adjustments to ensure that the electrode is centered. In addition to electrode being centered, it was important that there is a consistent cross-section between the copper tube and centering part. As can be seen above, there is a small gap between these two parts allowing water to flow in to refill the chamber while restricting water flowing backwards during an explosion. Spacers are also used in this design to help align the center

part. These spacers ensure that the part is not only concentric with the rest of the assembly but also horizontally fixed. The gaps in-between the spacers create inlets for the water to flow into the chamber. A flow analysis of this design can be seen below in Figure 18.

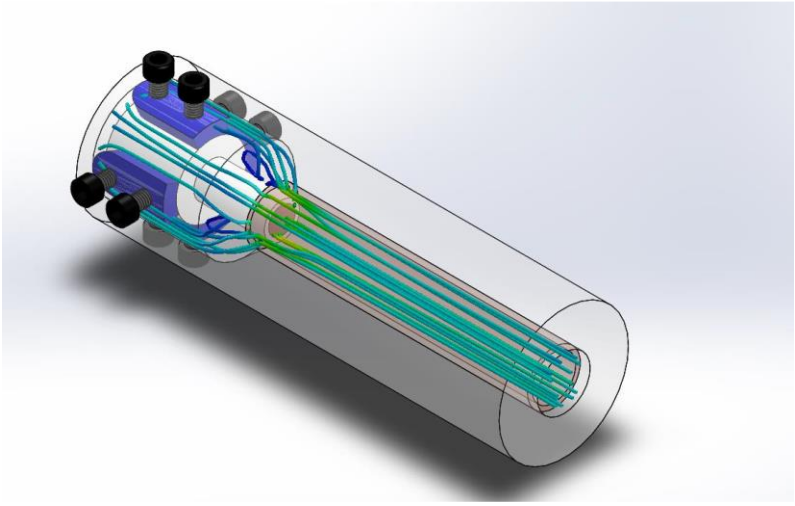

Figure 18: Mark III Explosion Chamber Flow Analysis

As can been seen in Figure 18 above, the design of this chamber allows for the constant flow of water from the inlet to the outlet (left to right in the figure above). The part of the chamber where there is a small gap between both electrodes does create some resistance of flow due to the small cross-section but it should be insignificant when filling the small volume of the chamber.

5.2.2 Testing & Results

To test the Mark III explosion chamber, it was attached to the fixuring assembly shown in Figure 16. However, when arcs were fired inside the chamber, there did not appear to be a directed thrust force or fog jet as in previous chamber versions. By using heavy-duty duct tape, the inlet end of the chamber was sealed, in order to mimic the configuration of the MkII chamber. Subjectively, this appeared to increase thrust force, as higher beam deflection and water movement were visible. The substantial pressures created by the explosion were sufficient to dislodge the duct tape from the inlet orifices.

As theorized by Dr. Graneau in "*Electrodynamic Seawater Jet: An Alternative to the Propeller?"*, the constant flow of water enables the water-arc thruster to function similarly to an MHD thruster, wherein Lorentz' force accelerates the current-carrying water out of the chamber. Graneau's design relies on the water-arc phenomenon only to strike the arc, ionizing the water and creating a low-impedance path. Once the arc has been struck, only a low power signal needs to be

applied in order to sustain thrust. The HV power supply described in section 3 provides $12kV_{rms}$ at 30mA. Based on previously conducted experimentation on MHD propulsion, 30mA would likely be too low of a current to prove useful. Additionally, the modifications to the discharge control mechanisms needed to implement Graneau's system would be very complex and costly. As such, the constant-flow design was abandoned in Mark IV

5.3 Explosion Chamber Mark IV

5.3.1 Design

After some poor initial results of the Mark III chamber, the next chamber was designed to only have one opening as with chambers MkI and MkII. The ring electrode design from the MkIII chamber was carried over and implemented in this chamber iteration. It was hypothesized that by having an electrode at the bottom of the chamber with another electrode lining the sides of the chamber, the electric arc created would create the fog from the water at the bottom of the chamber rather than leaving a small amount of water underneath where the explosion occurs. A cross-section of the CAD model of this new design can be seen in Figure 19 below.

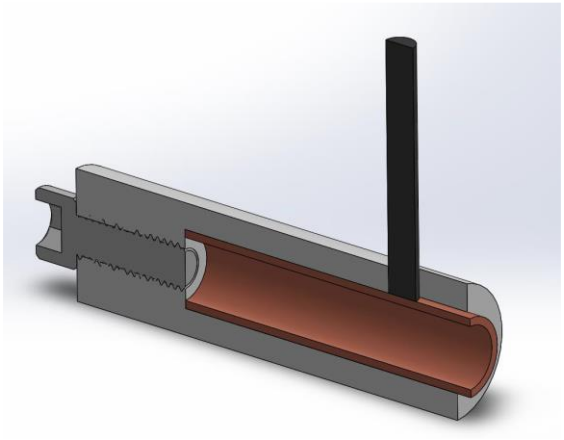

Figure 19: Cross Section of Mark IV Explosion Chamber

As can be seen in Figure 19, a copper tube is used for the outer ring electrode in the explosion chamber while a stainless-steel screw is used as the second electrode centered in the back of the chamber. The end of this screw is flush with the bottom of the chamber to ensure that the electric arc does not travel from the side of the screw to the outer electrode. This would not only be a shorter distance for the arc to travel but would also experience fewer losses due to its exposure to water.

The slot at the right end of the chamber was created to form an opening to solder the wire from the capacitor directly onto the copper electrode. The reason why the wire isn't soldered onto the end of the copper tube is to allow for a nozzle to be attached onto the end of the copper tube protruding from the UHMW plastic enclosure. The nozzle was added with the hope that by directing all the force though a small area more thrust could be generated. A CAD drawing of this explosion chamber with the nozzle can be seen below in Figure 20

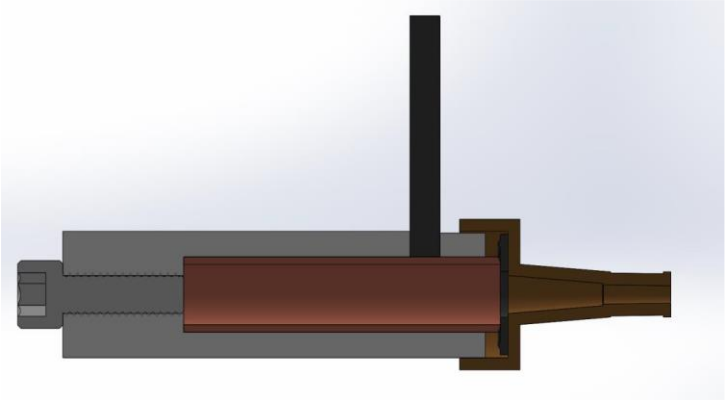

Figure 20: Cross Section of Mark IV Explosion Chamber with Nozzle

In order to securely attach the nozzle to the explosion chamber, the enclosure of the chamber was threaded to match the threads of the nozzle's flange. This ensures that the nozzle will not break off of the explosion chamber in the case that there is an extremely high pressure inside the chamber. A rubber O-ring is also used between the nozzle and the top of the copper tube. When the nozzle is screwed onto the chamber enclosure, the top of the copper tube is pushed onto the rubber O-ring forming a tight seal. This ensures that all of the pressure created from the water arc explosion is directed out of the nozzle. By having the nozzle attached with threads, it allows the team to design other nozzles in the future that are easily compatible with this explosion chamber design.

5.3.2 Testing & Results

While this chamber was intended for underwater use, the team tested it both in and out of the water to completely benchmark its performance. All of the tests were conducted by charging a single 2uF capacitor to 12kV and discharging it through the pneumatic switch used for the previous chambers.

For the tests conducted in the open air, the chamber was secured to a table using hose clamps. This ensured that the electrodes were completely isolated so there was no way to

accidently discharge the capacitor through a conductive part on the table. The first test was performed without a nozzle to benchmark the performance of the gen. 4 chamber compared to the previous chambers. The test also helped established a benchmark for when the nozzle was attached to the chamber. A series of images displaying water fog jet created by the test can be seen in Figure 21 below.

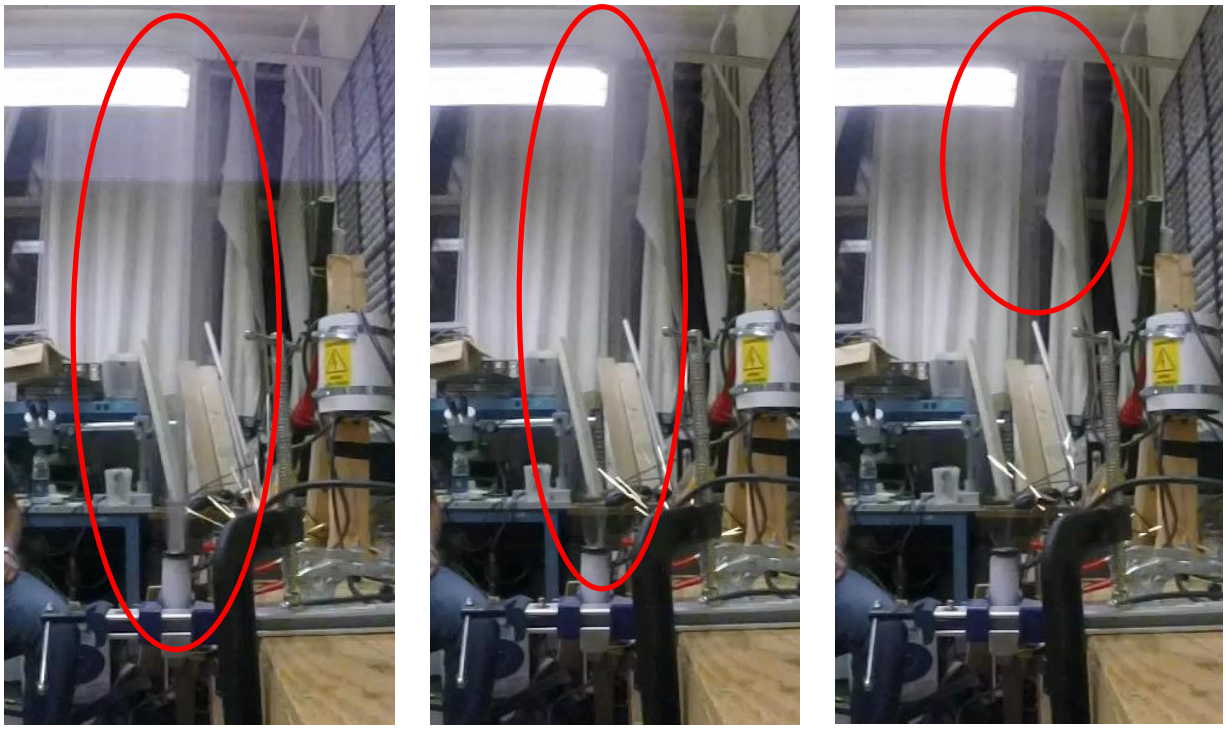

Figure 21: Chamber 4 open air water explosion test with no nozzle.

In the series of pictures above, each frame represents 0.016 seconds. The water fog jet is highlighted in each frame by the red oval. Since the water fog jet is composed a separated water particles traveling at high speeds, it can be difficult to record and usually is seen as a haze. That being said, the jet can be more easily seen in the frame on the left close to the outlet of the chamber. It was also noted that there was no remaining water in the chamber after the water explosion had occurred. This data was recorded and used as a benchmark for the following tests with a nozzle attached to the outlet of the explosion chamber.

In the next set of tests, the nozzle and O-ring were threaded onto the explosion chamber. In theory, the nozzle would create a high velocity exit water fog due to the smaller exit area. Due to the team's limited resources it was harder to determine if the water jet from the chamber was

accelerated by the nozzle however, it did appear that there was less of a fog jet than in previous experiments. A series of images can be seen below displaying the water fog jet created in this test.

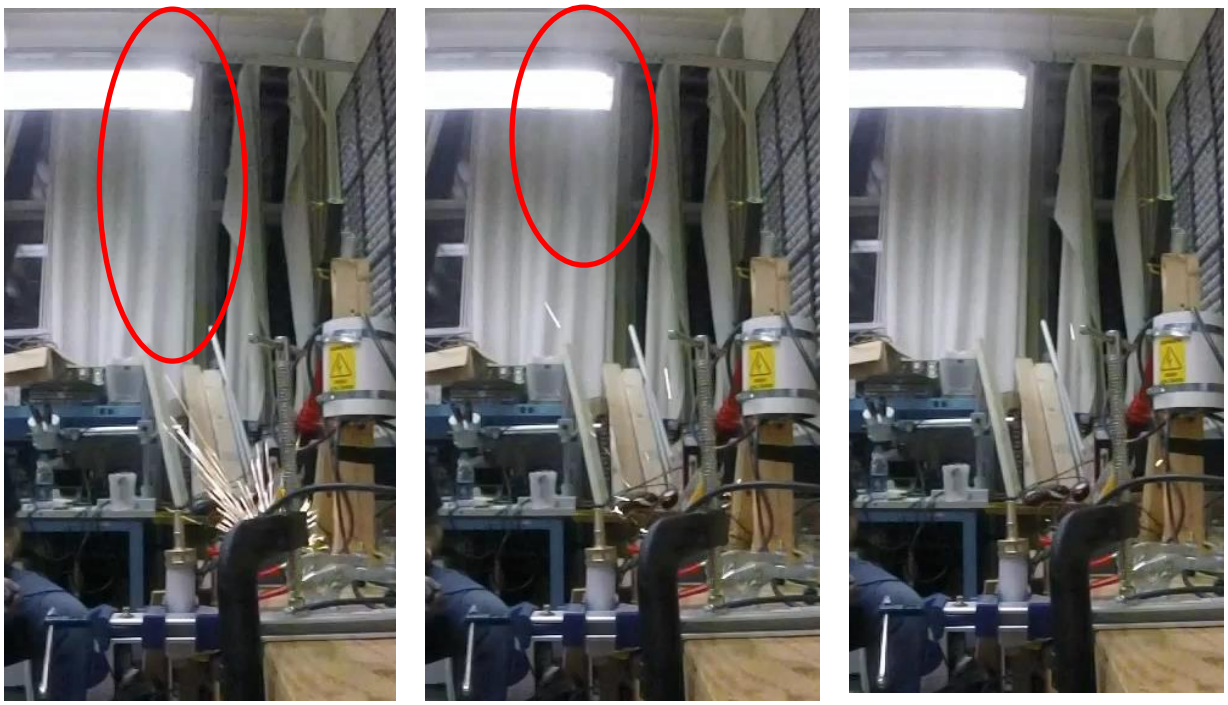

Figure 22: Chamber 4 open air water explosion test with nozzle.

In the figure above, the water jet created from the water explosion cab be seen in the region highlighted with the red oval. During the open air tests with the nozzle attached, the team notice that the water jet created was smaller than the benchmark water explosion conducted without the nozzle attached. The nozzle was the removed and the inside of the chamber was checked for any remaining water. In both tests conducted with a nozzle attached, water was found in the bottom of the chamber. Since there was no water left in the bottom of the chamber when there was no nozzle attached, this means that the water fog jet created with the chamber that had the nozzle attached were smaller than the benchmark water fog jet.

The team then switched to testing the chamber fully submerged both with and without a nozzle. In these tests, the explosion chamber was not restrained while underwater and was instead laid on the bottom of the tank with the high voltage transmission wires draped over the side of the tank. By allowing the chamber to move freely underwater, the thrust force of the chamber could be visually seen by the distance that the explosion chamber travels. In the first test, the nozzle was removed from the chamber to benchmark the chamber's performance underwater. Once that was

complete and the nozzle was attached, the chamber was submerged for second test. In this test however, when a water arc explosion was created, the snout of the nozzle was blown off the threaded portion of the nozzle. While the snout of the nozzle initially press-fit onto the threaded body of the nozzle, this test showed the water explosions due create a significant amount of pressure inside the explosion chamber. A series of frames taken from a high speed video displaying the nozzle breaking can be seen in Figure 23 below.

Figure 23: Still frames from chamber 4 underwater test during which the nozzle broke.

The frame on the left and right are taken one frame before and after the water explosion occurred. As can be seen, immediately after the water explosion took place, the snout of the nozzle had been blown out of the body of the nozzle. This shows that there is a significant amount of pressure created inside the explosion chamber to be capable of separating the snout from the body of the nozzle. A possible explanation for why the snout of the nozzle didn't blow off in the open air tests is that in the open air tests, the chamber was filled with air, a compressible gas, whereas when the chamber was submerged, it was filled with water, an incompressible fluid. With the outlet at the end of the nozzle being as small as it is, the flow of water out of the nozzle may have been restricted resulting in a high water pressure, forcing the snout of the nozzle off of the body.

Following this test, the threaded body of the nozzle remained attached to the end of the chamber to see if there were any performance increases when using a larger diameter outlet. After a few tests were performed, there were no noticeable increase in performance over the tests done without the nozzle. However, during the tests without the nozzle, the team noticed that the copper tube that was press-fit inside the UHMW enclosure was pushed out roughly 2 or more mm each time a water arc explosion was fired. This brought up the concern that the chamber would not be rigid enough to withstand multiple arc while on the boat.

5.4 Conclusions & Final Design Selection

After the team constructed and tested each of the previous four unique chamber designs, the team was able to determine exactly what features should and should not be included in the final chamber design. To easily compare the tests results from the sets of experiments performed on each chamber, a comparison table was built. This table can be seen in Table 1 below.

Table 1: Table comparing the experimental results of each explosion chamber revision.

Chamber Revision	Discharge Circuit	Successes	Failures
Chamber 1	• 10kV • 1uF Oil filled Capacitor • Pneumatic Switch	• Durable stainless steel concentric chamber	• Press-fit UHMW Plastic plug
Chamber 2	• 12kV • 2uF Polypropylene Film Capacitor • Pneumatic Switch	• Durable UHMW enclosure • Excellent mounting capabilities	• Brass electrodes deteriorated quickly • Electrodes not flush with the bottom of the chamber potentially decreasing chamber performance
Chamber 3	• 12kV • 2uF Polypropylene Film Capacitor • Pneumatic Switch	• Durable copper electrode • Durable concentric brass ground electrode	• Inlet allowed backflow of water explosion pressure (decreasing performance)
Chamber 4	• 12kV • 2uF Polypropylene Film Capacitor • Pneumatic Switch	• Stainless Steel screw used as ground electrode • Durable copper electrode	• Copper tube electrode pushed out of UHMW enclosure after each water explosion • Hose nozzle decreases the performance of the explosion chamber

This table provided the team with a quick comparison chart for all the chambers so the best configuration could be easily determined. For the electrodes, the team had the most success with chambers that had concentric electrodes rather than two points like in chamber two. It was also determined that the electrodes would not be constructed out of brass due to the amount of degradation to the electrodes in the second chamber design. Instead, the electrodes would be constructed using stainless steel and if need be aluminum.

From the testing done with chamber four where the inner electrode was being slowly pushed out, the team determined that the final electrode should threaded into the chamber enclosure to insure that the chamber assembly would be as rigid as possible. Finally, the team also determined that the chamber should consist of only one outlet and no inlet. From the tests conducted with chamber three, the team noticed that the performance of the chamber was severely impacted by the chamber's inlet. With the final chamber design being a pulse jet, only having one outlet would direct all of the thrust in one direction, minimizing any loses in the chamber. By implementing all of these design criteria, the life of the chamber would be greatly increased from the previous chamber designs and make it more reliable for repeated use in a boat.

6. The WAEV-1

The Water-Arc Explosion Vessel – 1, or WAEV-I is the culmination of the work to produce a water-arc thruster detailed in the previous sections. It is intended to showcase the potential for water-arc propulsion, and to provide a tangible demonstration of the vast power that can be obtained by proper application of water-arcs. The WAEV-I was constructed once sufficient preliminary research and experimentation had been conducted, and implements the resulting designs. Some final design modifications were made prior to construction, in order to optimize the water-explosion apparatus for on-vessel application.

6.1 Power Supply Adaptation

When deciding how to adapt the power supply for the WAEV-1 vessel, two options were clear. Either redesign the power supply to be much smaller and run on batteries or to continue to use the current power supply and by running power lines to the boat. Considering that no small power supply designs, which could supply a high enough current, were found it was decided to adapt the neon sign transformer for use with the WAEV-1. These adaptations sought to make the power supply more portable and able to charge the capacitors quickly

The neon sign transformer outputs a 17kV peak voltage AC waveform. The previous power supply used two high voltage diodes, in series, to rectify the output waveform. While this half-wave rectifier could be used to charge the capacitors, only half the delivered power was being utilized. In order to use the full power output and decrease the charging time of the capacitors, a full-wave rectifier was needed. Four high voltage diodes were purchased and used to create a full-wave rectifier. This addition to the power supply decreased the charging time of the capacitors by about half.

The charging resistors used in prior experiments were fairly large since the capacitor did not need to be charged quickly. With the full-wave rectifier active, the capacitors could be charged to 10kV in close to 5 seconds. The ideal charging time was decided to be 1.5-2 seconds given the limits on how quickly the capacitor should charge and be discharged. In the final boat design two 2uF capacitors were being used to create greater propulsion. Using the time constant and charging equation for these capacitors, a resistance of .5 MΩ was selected. Two 1 MΩ high wattage resistors put in parallel to get this resistance. When this new resistance was used the charge time was within the ideal charging time range.

Since the WAEV-1 was going to be tested in a body of water and not a controlled laboratory environment, the final design of the power supply needed to be very portable and contained. An old two level hand card was found and used for this purpose. The bottom level of the cart was used to hold the NST, the full-wave rectifier, and the high voltage connection ports leading to the boat. Each component was firmly attached to the cart using hardware and adhesive. As in the previous test the high voltage, voltage probe was connected to the positive high voltage connection terminal. The upper level of the cart was used to store the power system controls and monitoring equipment. The variac voltage control unit was fixed to the cart and used to control the voltage to the NST on the bottom level. The DMM used to monitor the voltage on the capacitors was also on the top level and connected to the voltage probe on the bottom. The minimal usage of the top level allowed for the boat to be transported on top of the cart. Finally the high voltage emergency discharge stick was also incorporated into the design on the side of the cart, where it was readily accessible. This design proved to be highly portable, and provided easy access to the controls and monitoring systems, while shielding the operator from the high voltage components.

6.2 Discharge Circuit Revisions

To increase the firing frequency of the explosion chamber, two 2uF capacitors would be used to double the firing rate compared to a single capacitor. This doubled firing rate would be accomplished by charging the capacitors simultaneously, but 180 degrees out of phase. This phase shift allows one capacitor to remain charging while the other creates a water arc explosion allowing the firing rate to be doubled. The plot seen below in Figure 24 displays the alternating charging cycle of the two capacitors.

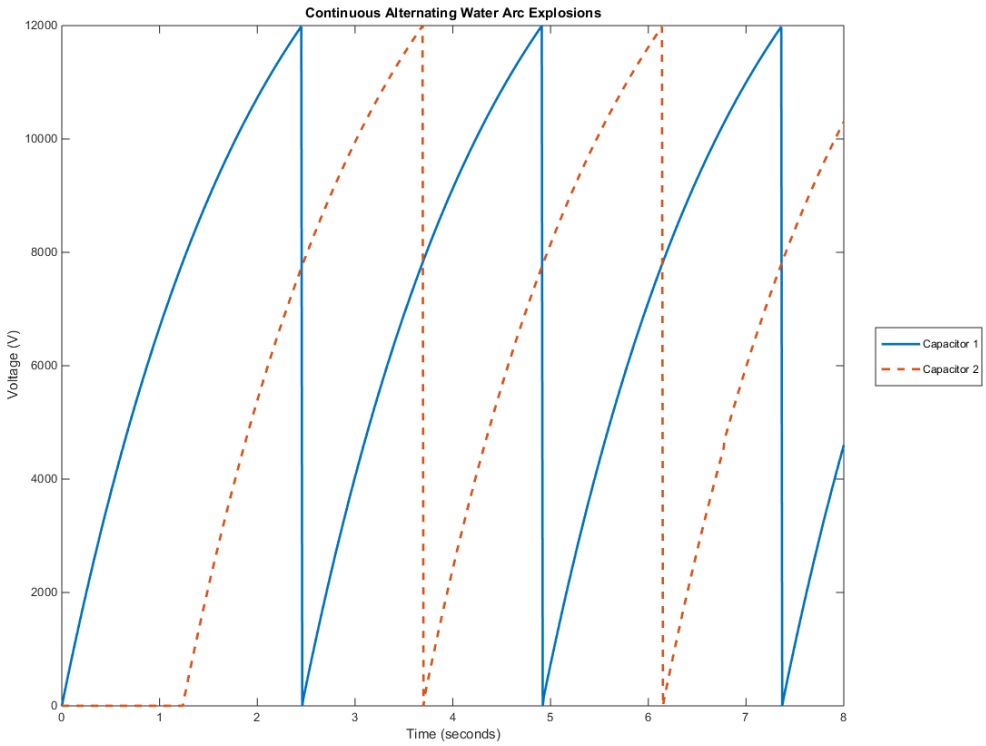

Figure 24: Plot of Voltage in Capacitors 1 and 2 of a continuously charging and firing system.

As can be seen in the figure above, once the capacitor reaches a voltage of 12000 Volts, it is immediately discharged through a water arc explosion and then starts recharging shortly after. By charging the capacitors using this method, the charging current stays at a relatively stable rate over the course of the charging cycle.

While this method does increase the frequency of water arc explosions, it results in a complex circuit with many switches. The reason for a large amount of switches is because the capacitors cannot be connected to the explosion chamber while charging and especially not when another explosion chamber is creating a water arc explosion. A schematic detailing a possible solution for this circuit can be seen below in Figure 25.

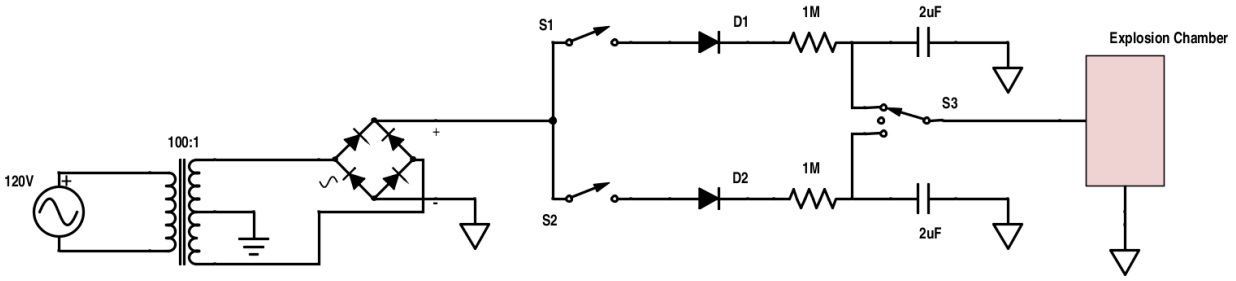

Figure 25: Schematic of Alternating Firing Circuit

In order to reduce the large number actuators required for the switches seen in the schematic above, a series of double pole, single throw (DPST) switches were designed to simplify the controls. This was accomplished by modifying the output of a servo arm to have a contoured plate of mica. Mica was the material of choice in this application due to its extremely high dielectric strength. This way, when the switch was in the off position, the mica plate would be placed in between to carriage bolt heads creating an open circuit. However, when the switch was turned on, the mica would simply lift out from in between the two bolt heads allowing them to arc from one to another creating a closed circuit. An example model of this design can be seen below in Figure 26.

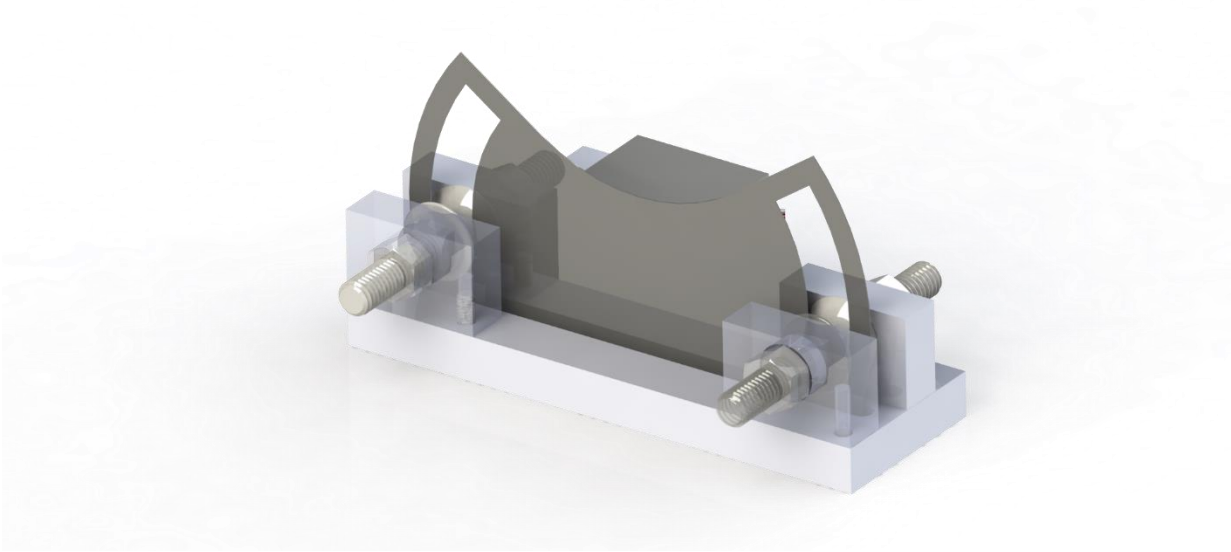

Figure 26: Rendered of DPST Switch.

As can be seen in the figure above, depending on the position of the mica plate there can be three possible switch settings: both switches on, switch one on and switch two off, or switch one off and switch two on. It is possible for there to be a position of the mica plate where both

switches can be off, however, in order for the mica plate to get into that position, it could potentially have to go through another setting before reaching the both off position.

The mechanics of the switch were not the only issue however. Due to the high EM created by the high voltage, there was a large amount of interference within the entire system's electronics. In some cases the Arduino microcontroller that was being used to control the switches would shut down and in other cases the servo arm would move or jitter without any control signal. This caused the entire system to become unreliable and thus a safety hazard.

In an effort to simplify the switch designs, the team designed other switch solutions in the place of the double pole, single throw servo switch mentioned above. All of these switches however, were single pole, single throw (SPST) switches, thus requiring more electronics. The first switch concept took the idea of using two bolt heads with a plate of mica in the middle as a switch but replaced the servo motor with a linear door-lock actuator from a car. This worked by attaching a piece of mica onto the end of the door-lock actuator which would then move the mica plate in and out of the area in between the bolt heads creating a switch. A 3D model of this switch can be seen in the model below in Figure 27.

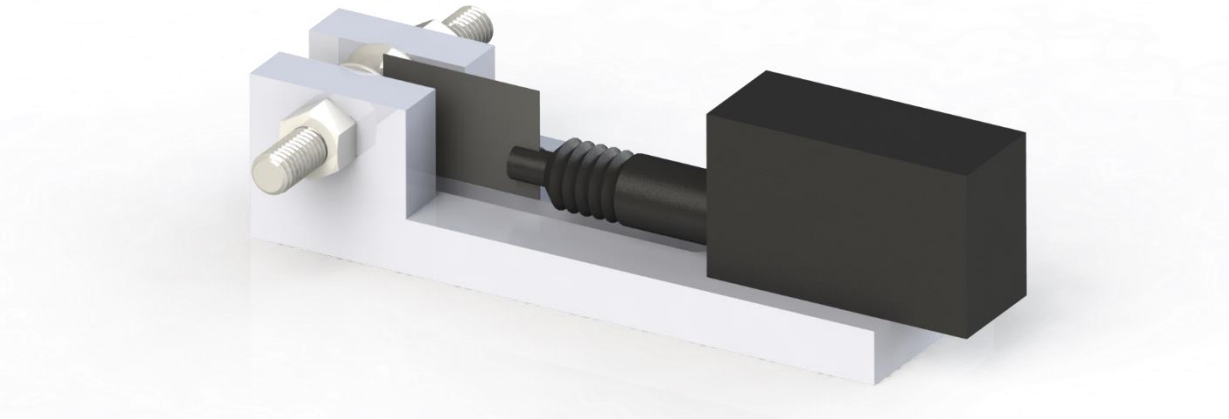

Figure 27: Door lock actuator SPST switch design.

In the team's final electronic switch revision, the power loss of arcing through air from one bolt to another was reduced by having the electrodes in contact with each other while in the on position. In the off position, a plate of mica would be pushed in between the two electrodes creating an open circuit. This design concept was accomplished by having the two electrodes spring loaded against each other. This way while in the off position, the two electrodes would just be pushed up

against the mica plate creating an open circuit. However, as soon as the mica plate is removed, the electrodes spring back together creating a closed circuit. In the model seen below in Figure 2728, the electrodes are made from copper to reduce the risk of accidentally welding the electrodes together when a water explosion is fired.

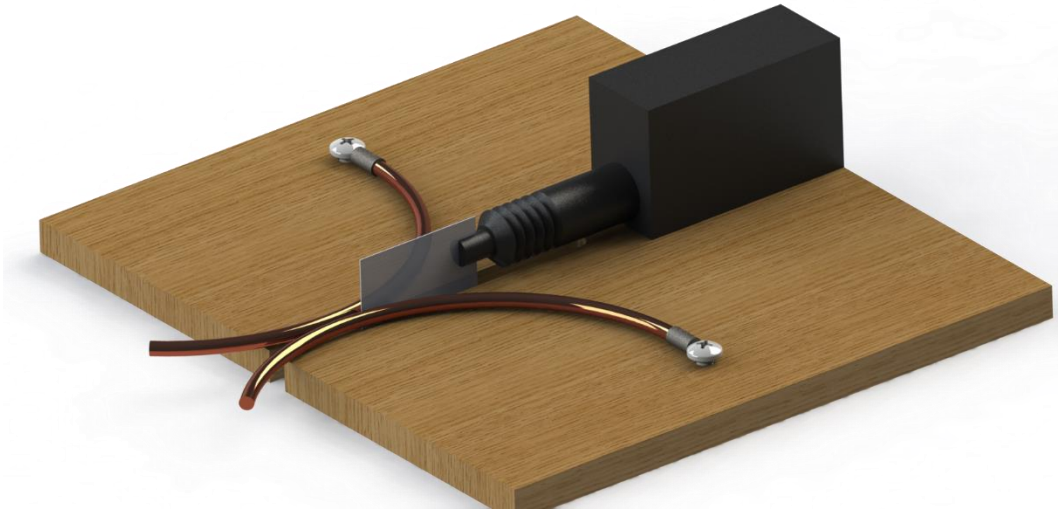

Figure 28: Copper wire spring SPST switch with door lock actuator.

Similar to the DPST switch mentioned above, all of the electronic SPST switches ran into the issue of EM interference from the high voltage. To rectify this problem, extensive shielding was purchased to isolate all of the electrical components from the EM interference. The wires to the servo were fed through a plastic and grounded copper wire sleeve (McMaster part #6971T13). A 7V zener diode was also added to each servo wire to short any voltage surges to ground that could have been potentially interrupting the signal to the servo. In addition to this, all of the microcontrollers were housed in a grounded aluminum enclosure. This created a Faraday cage around all of the electrical components, shielding them from any EM interference. The servo motors and door-lock actuators were also wrapped in grounded aluminum foil to increased shielding on the electronics inside. Even with these methods of shielding, the EM interference still persisted causing serious problems with the microelectronics. It was mainly due to these problems that the idea of using an electronically controlled switch was abandon and the team focused on designing a purely mechanical switch with no electrical components.

6.2.1 Seperate charging and firing (separate chambers)

Due to the complexity of the circuit to accomplish alternate charging and firing cycles, the team decided to try the idea of having two explosion chambers, each with their own capacitor. The capacitors would be charged separately with no linked components, requiring two neon sign transformers. A schematic of the circuit can be seen in Figure 29 below.

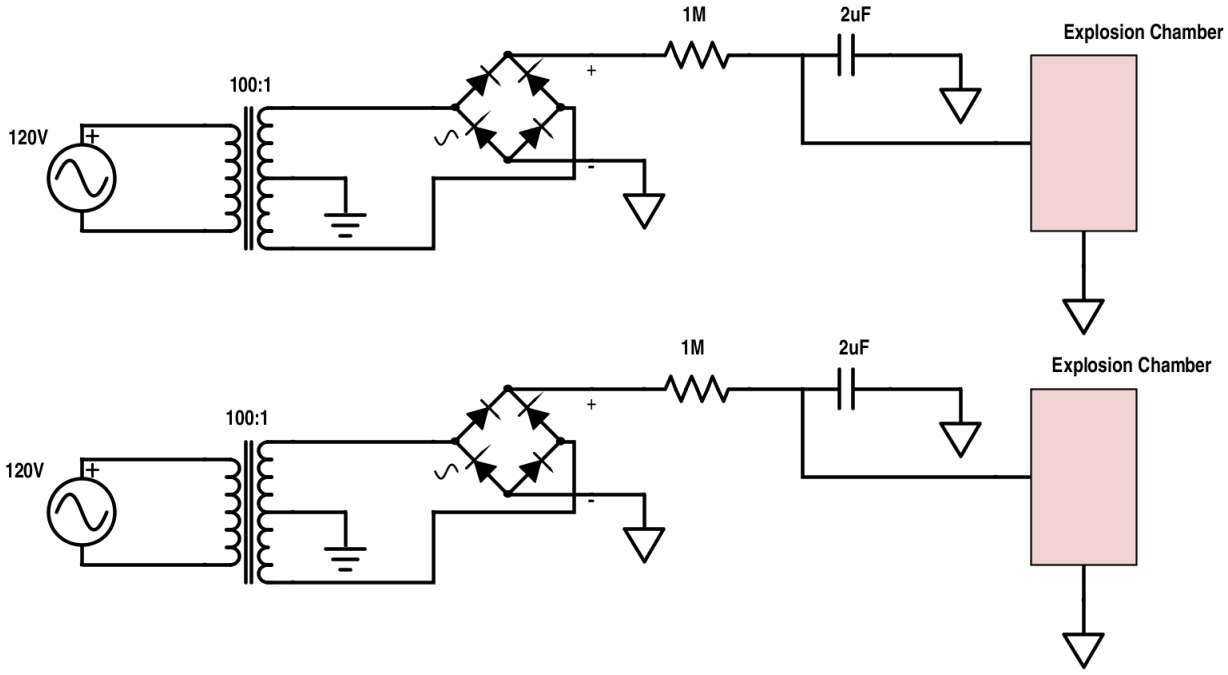

Figure 29: Schematic of dual explosion chamber circuit.

This circuit could be configured to either have the explosions chambers create water arc explosions at the same time or alternate at half of the period of one chamber. While this could increase the power output of the system, the team had some concerns about the stability of the boat and the force from the water arc explosions turning the boat rather than pushing it directly forward.

In this water arc explosion system, the team focused on designing a mechanical switch with no electrical components. With this in mind, the team designed a solid-state mechanical switch called a spark gap. In this switch, there are two carriage bolt heads, used for their uniform, domed shape, that are positioned at a predetermined distance. When the voltage potential across the spark gap is large enough for an arc to be created, the switch “turns on”, allowing electrical current to travel through the switch. Using the conductivity of air, our team was able to easily calculate the distance needed between the electrodes of the spark gap to generate an arc, automatically “turn on” the switch at any voltage. A 3D model of this switch can be seen below in Figure 30.

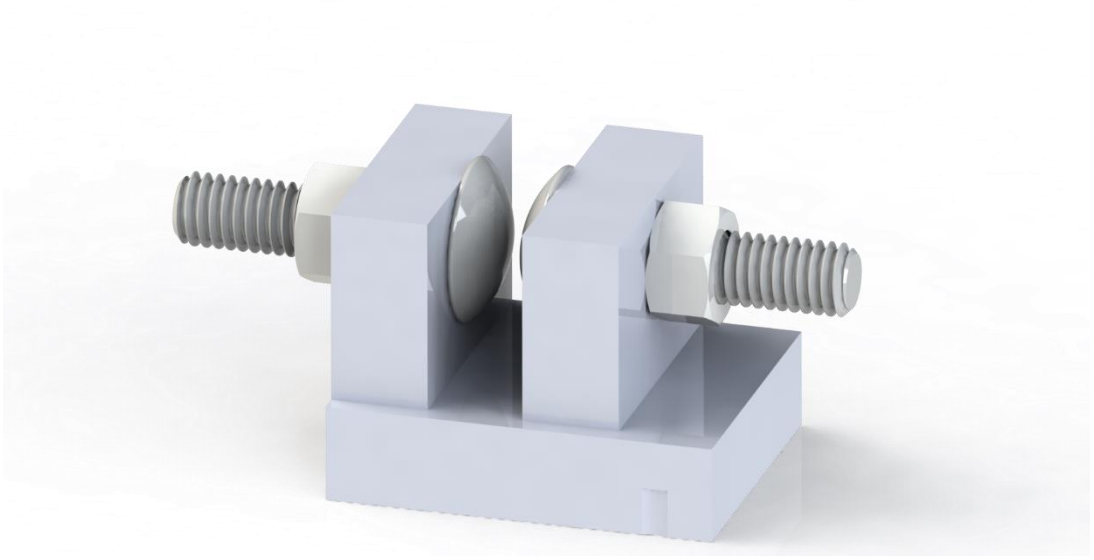

Figure 30: Spark gap switch design.

A main issue that was found with the spark gap was that while the switch would perform routinely well, the voltage at which the spark was created was difficult to tune. In some cases, it appeared that the voltage at which an arc was created differed by 100Volts at times. This raised some concerns about the ability to be able to have two chambers fire at the exact same time without the use of electronics. It was feared that even if the spark gap for each chamber where tuned to be the exact same distance apart, the arc could possibly occur at slightly different times. The team felt that the variability in firing could affect the boat's performance and began to look back into the idea of using a single chamber.

6.3 Final Electrical Design

Taking the knowledge that the team had gathered from designing the previously mentioned electrical systems, the team came to the conclusion that it was best to use a single chamber with both capacitors in parallel. In this design, the capacitors are charged at the same time and can actually be modeled as a 4uF capacitor. In order to keep the time constant of the capacitor the same, another 1MΩ resistor was placed in parallel to bring the equivalent resistance down to 500kΩ. A schematic of the final circuit can be seen below in Figure 31.

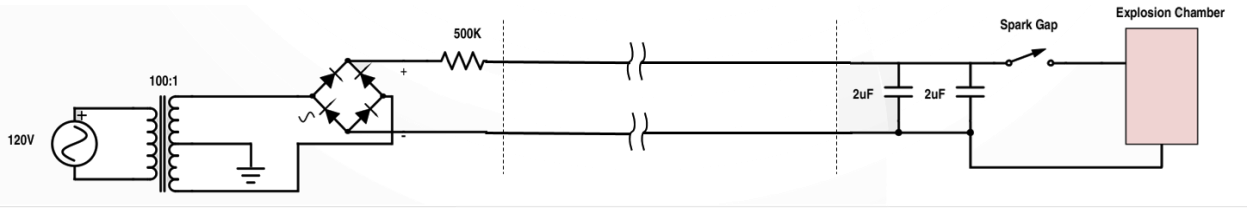

Figure 31: Schematic of final water arc explosion circuit.

By adding the additional capacitor in parallel, the energy output was doubled leading to even larger water arc explosions. The use of a single chamber also allowed the thrust from the water arc explosions to be directed at the center of the boat, keeping the boat from turning. To charge the capacitors, 120V at 60Hz signal from a wall outlet was transformed using the neon sign transformer to be 12kV at 60Hz. This AC signal was then rectified to a 16920V DC signal using a full-wave rectifier. This DC signal was then used to charge the capacitors at their maximum charging rate allowing the team to reach 8kV in roughly 1.6 seconds.

After having success with the spark gap switch, the team choose to use it as the triggering switch in the final design. The distance between the electrodes where adjusted to be 3.2mm apart, enough for roughly 8.5kV to arc across it. This voltage would allow for large water explosions to occur while still having a rapid firing rate.

6.4 “Vaka” Design

The WAEV-I is intended to be a means of demonstrating the innovation of water-arc propulsion. Thus, the vessel itself was designed with the goal of simplicity in order to facilitate rapid completion, as well as to minimize the challenges commonly faced in marine vessel construction. A multihull design was chosen to facilitate vessel stability even under uneven loading. Such designs were pioneered by the indigenous people of Polynesia, who constructed multihull canoes. These consisted of a center hull called the “vaka” and at least one outrigger, called an “ama”. These hulls were connected by rods or poles known as “aka’s”. A three-hull, or trimaran design was chosen for the WAEV-I, consisting of a vaka and two ama’s, connected by two aka’s spanning between the ama’s. The vaka houses all the electrical components, as well as the water-arc thruster, while the ama’s are intended solely for balancing, similar to training wheels on a child’s bicycle. Thus, the ama design was completed after the vaka was constructed.

The vaka was designed to support the weight of the electrical and propulsion components, as well as the hull itself. Which was estimated to be around 10kg. Thus, the total water

displacement was required to be 10 liters. The dimensions of the hull were chosen to provide this water displacement, and the hull was modeled in Solidworks. After the vaka was modeled, the fluid displacement was verified in Solidworks, and hull speed calculations were performed to ensure the hull design wouldn't limit the thrust of the propulsion system. The hull speed is given by the following equation.

$$v_{hull} = 1.34\sqrt{L_{wl}}$$

Where v_{hull} is in knots, and L_{wl} is the length of the waterline in feet, equal to 9ft for the WAEV-I vaka. The vaka was determined to have a hull speed of 4.02 knots, which exceeds the expected speeds achievable with the designed propulsion system. Following hull design validation, cutouts were modeled into the vaka for mounting the capacitors and water-arc thruster. To mount the capacitors, a section of 6" Sch. 40 PVC half-pipe was installed into the vaka. An acrylic panel is fixed to one end of the PVC pipe to distribute thrust forces, and also contains an M8 clearance hole for securing the capacitors. In order to allow water access to the explosion chamber, a 1" ID hole is included on the back face of the hull, below the waterline. A CAD model of the final vaka design can be seen in the figure below.

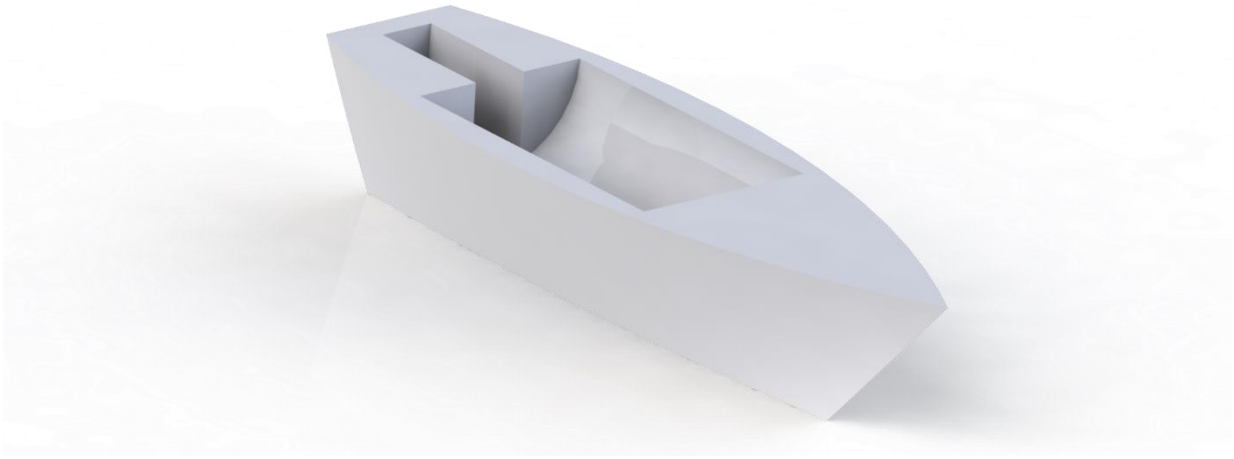

Figure 32: CAD Model of vaka

6.5 Water-Arc Thruster Design

6.5.1 Design Objectives

Optimal design of the water-arc thruster system required implementation of experimental results obtained during previous research. During the course of this experimentation, variations in chamber diameter, electrode configuration, and manufacturing methods were shown to affect the

explosive force of the water-arc explosion. These characteristics were optimized on the final design of the water-arc thruster. In addition, the water-arc thruster system is designed to be triggered by a spark-gap switch. To minimize power loss in the high-current discharge leads, this switch should be placed as close as possible to both the explosion chamber and the storage capacitors. The final design of the water-arc explosion system must facilitate this. Finally, the explosive forces generated during the water-arc explosion were shown to destroy what were thought to be excessively robust devices. After conducting several water-arc explosion experiments, the explosive forces are better understood, allowing for implementation of sufficiently robust designs and manufacturing methods on the final water-arc thruster.

6.5.2 Chamber Design

The objectives outlined in the previous section guided the design of the final WAEV-I thruster system. A rod-and-ring electrode configuration was shown to produce the most forceful underwater explosions, as demonstrated by the Mark IV explosion chamber. Thus, a rod-and-ring configuration was also used on the final design. The rod electrode was realized in the form of a ¼-20 stainless steel machine screw, positioned flush with the explosion chamber, which also serves the purpose of the ring electrode. The explosion chamber was machined from a 1” 316 stainless steel rod, which was bored with a 5/8” insert drill. An ID of 5/8” was chosen to match the ID of the Mark IV explosion chamber. A UHMW block was machined to accept the explosion chamber and ground electrode, and included threaded holes for mounting to the WAEV-I hull.

The explosion chamber is fixed to the mounting block via a UNF 1”-13 external thread cut into the OD of the chamber, and tapped into the UHMW block. This ensures a rigid and secure connection, capable of withstanding the high stresses exerted by the water-arc explosions. A nitrile O-ring is placed between the chamber and the mounting block to provide a high-pressure seal, ensuring that maximum explosive force is directed out the chamber orifice. Silicone caulking was applied to any wet-dry interfaces to prevent the accumulation of bilgewater. As can be seen in the model above, the thruster system minimizes the length of high-current discharge leads by integrating the spark gap switch and capacitor mounting hardware into the thruster assembly itself. A rod threaded into the UHMW block contacts the ring electrode, and terminates in a stainless steel cap nut electrode. An aluminum plate attached to the capacitor mounting rod is positioned above the cap nut electrode, completing the spark gap. The gap is adjustable by varying the position of the retaining nuts on either side of the aluminum plate.

6.6 Final Design of the WAEV-I

Following the completion of the design of the center hull and the water-arc thruster system, the final design was completed by integrating these two components, and adding the ama's and aka's. A rendering of the final design of the WAEV-I is shown in Figure 33 below.

Figure 33: Rendering of the final design of the WAEV-1.

The ama's were designed to provide minimal drag, while supplying enough support to ensure ship stability. Closed-cell foam was chosen as the optimal material for the ama's as the foam would prevent them from sinking. The aka's were to be made from 1/8" steel flat bar, and dimensioned such that the bottom of the outriggers were just beneath the vaka waterline. In addition, the ductility of the steel aka's was intentionally preserved during fabrication, in order to allow them to be bent to adjust ama height.

6.7 Manufacturing the WAEV-I

6.7.1 Vaka Construction

To facilitate timely fabrication, great care was taken during selection of manufacturing processes. In terms of hull construction, the vaka requires a higher level of precision than the ama's, since all other components will be mounted to it. To ensure that the dimensions of the vaka match the designed dimensions, a foam core was constructed from ½" thick laser-cut closed-cell

polystyrene insulation panels. The process of creating drawings for the individual panels from the 3D Solidworks geometry was automated by a software tool called Autodesk 123D Make. The foam core was assembled from the panels using 3M Super 77 Spray Adhesive. An image of the foam core of the vaka can be seen in Figure 34 below. Note that the vaka is placed upside-down on the workbench in the picture.

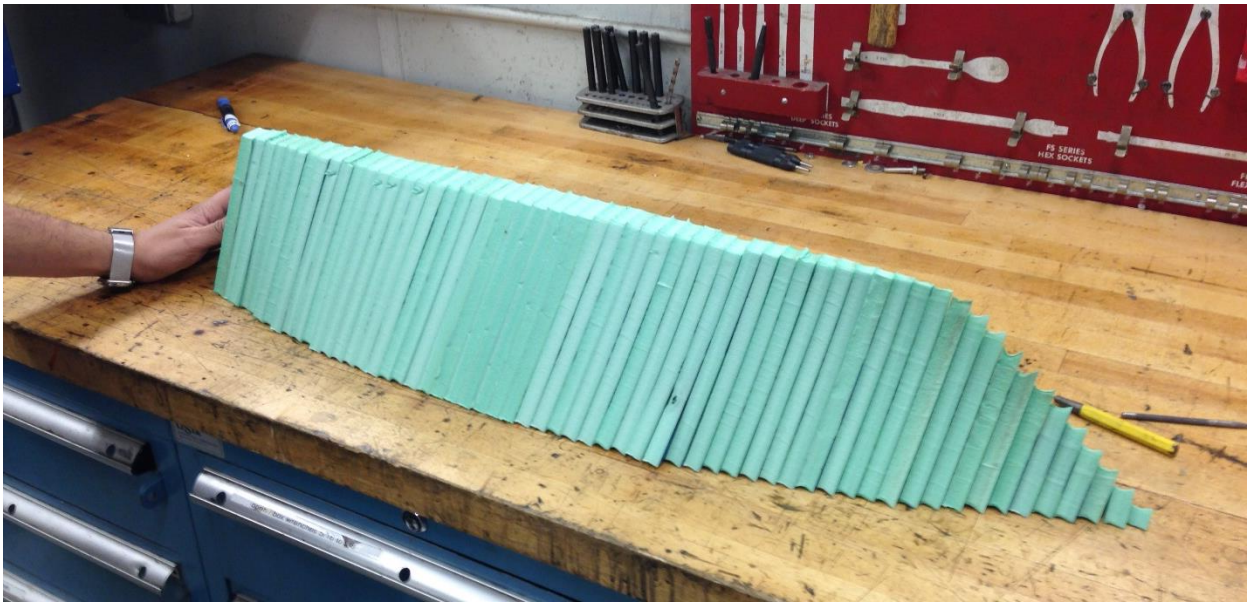

Figure 34: Foam hull placed upside-down on a workbench.

Once the spray adhesive had fully cured, the foam core was complete. At this stage, while the foam core clearly resembled the designed shape of the vaka, the ½" resolution of the slices significantly detracts from both the aesthetics and the hydrodynamics of the hull. To solve this issue, 3M Bondo brand talc-based auto body filler was applied between the foam panels, smoothing out the exterior surface. Once cured, the filler was sanded to a smooth, uniform surface, using a maximum grit of 220. Figure 35 shows an image of the vaka after application and sanding of the body filler.

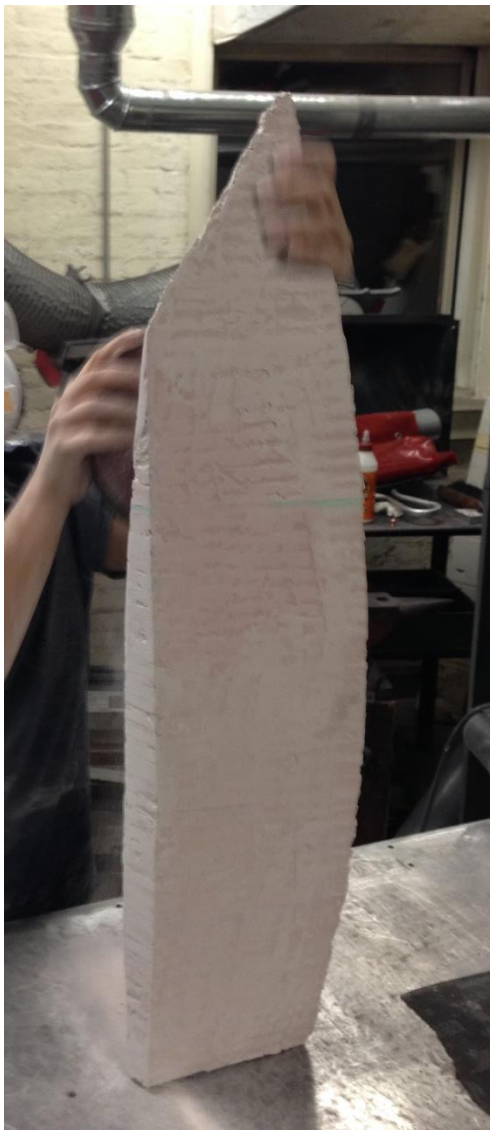

Figure 35: Vaka hull after sanding Bonda body filler.

To ensure water resistance, as well as to provide an excellent mechanical barrier, several layers of fiberglass were applied to the vaka. To promote secure adhesion, a Brillo pad was used to abrade the Bondo-covered surface prior to cleaning with an isopropyl alcohol solvent. Sheets of woven fiberglass cloth were applied to the prepared surface, and adhered with polyester resin. Three layers were applied in a ventilated room at an ambient temperature of 73^{o}F, and allowed to cure overnight. An image of the hull after application of fiberglass cloth is shown in Figure 36 below.

Figure 36: Vaka hull after application of fiberglass cloth and resin.

After the fiberglass had been sanded until smooth, the hull was prepared for painting. Two coats of primer were applied to the fiberglass surface, followed by several coats of Rustoleum Marine Topside paint. Once cured, the hull construction was complete.

6.7.2 Thruster Fabrication

The WAEV-I's water-arc explosion thruster was fabricated from stainless steel and UHMW. Contours for the PVC pipe and ground electrode access, as well as holes for the spark gap, explosion chamber and capacitor mount, were CNC machined into the UHMW block. The capacitor mount was made from two sections of Grade 8 steel threaded rod, mitered and welded at a 90 degree angle. The 1"-13 threads were cut into the 316 stainless steel chamber using a carbide die. Once the parts were machined, the chamber, ground electrode, and capacitor mounts were inserted into the UHMW block. A section of threaded rod was inserted into a second threaded hole in the UHMW, making contact with the ring electrode. At the interface between the rod and the electrode, silver epoxy was applied to increase conductivity. To complete the thruster assembly, the aluminum spark gap plate was installed on the capacitor mount, prior to silicone caulk application.

6.7.3 Ama and Aka Construction

While the foam core method used for the construction of the vaka did yield dimensionally accurate results, the labor intensive process was not necessary for ama construction. Instead, two polystyrene foam airplanes, were purchased, and the fuselage was used as a blank for each ama.

Figure 37: Foam fuselage being cut with a hot wire foam cutter.

In Figure 37, the foam fuselage was further shaped on a hot-wire foam cutter, to match the designed shape. These were then wrapped with fiberglass cloth and polyester resin. The ama's were painted in the same manner as the vaka. #10 clearance holes were drilled through the ama's to serve as mounting points. To mount the ama's to the vaka, two steel aka's were constructed from 1/8" thick flat bar. The ID countour of the PVC capacitor cradle was bent into the bar, before two right angles were added with a flange for mounting to the ama's. As the mild steel used to make the aka's is prone to corrosion, the aka's were coated with gold Valspar spray paint.

6.7.4 Final Assembly

A PVC capacitor cradle was constructed by sawing a section of Sch.40 PVC pipe in half. Then, an acrylic panel was laser-cut to conform to the OD of the pipe, and to include a mounting hole for the capacitor. The panel was attached to the PVC pipe with a series of #8-32 machine screws, as well as epoxy resin. The thruster assembly was inserted into the cutout in the vaka, such that the explosion chamber protruded past the hull ½". The PVC capacitor cradle was secured to the foam cutouts in the vaka with construction adhesive and fixed to the thruster assembly with ¼-20 machine screws. The aka's were screwed into the PVC cradle before the ama's were installed, and their height was adjusted by bending the steel aka's. To protect the upper foam surface of the vaka, as well as to increase aesthetic appeal, a series of opaque black acrylic panels were laser cut to form a cover over the top surface of the vaka. The panels were cut in five sections, and adhered to the foam with construction adhesive. Finally, the wiring between the capacitors and the thruster was completed, and tether cables were installed. The image below in Figure 38 shows the WAEV-I after assembly.

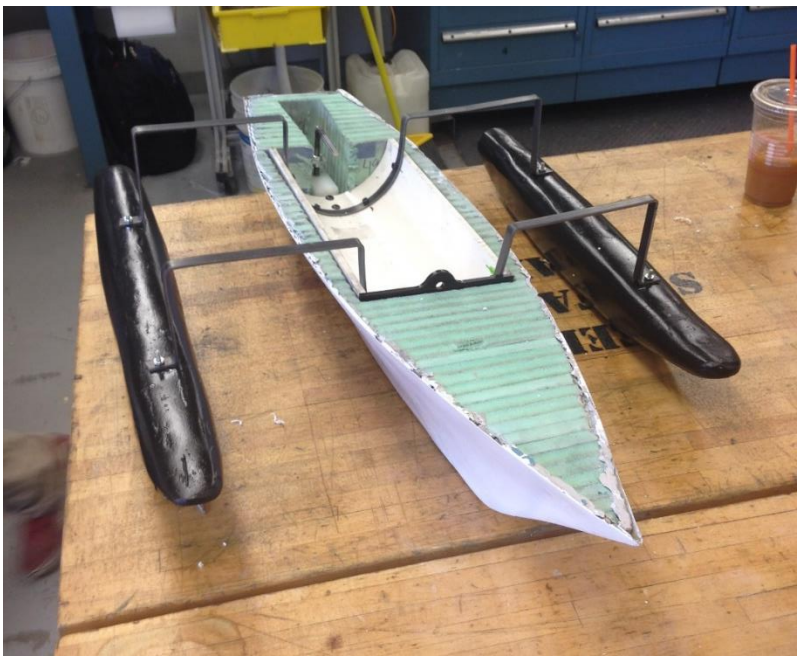

Figure 38: WAEV-1 in the midst of initial assembly process.

6.8 Initial Testing and Results

The WAEV-I was tested in the WPI Rowing tanks, due to their limited turbulence, as well as the dimensions. The WAEV-I was outfitted with a GoPro Hero 3 camera, oriented to capture

video of the thruster assembly during operation. The control cart described earlier in this section was placed on the deck, and the HVDC tether cables were placed in the water, along with the WAEV-I. Initial tests were intended to verify the functionality of the WAEV-I, as well as to confirm that the vessel is able to achieve motion. The image below in Figure 39 depicts the WAEV-I's maiden voyage.

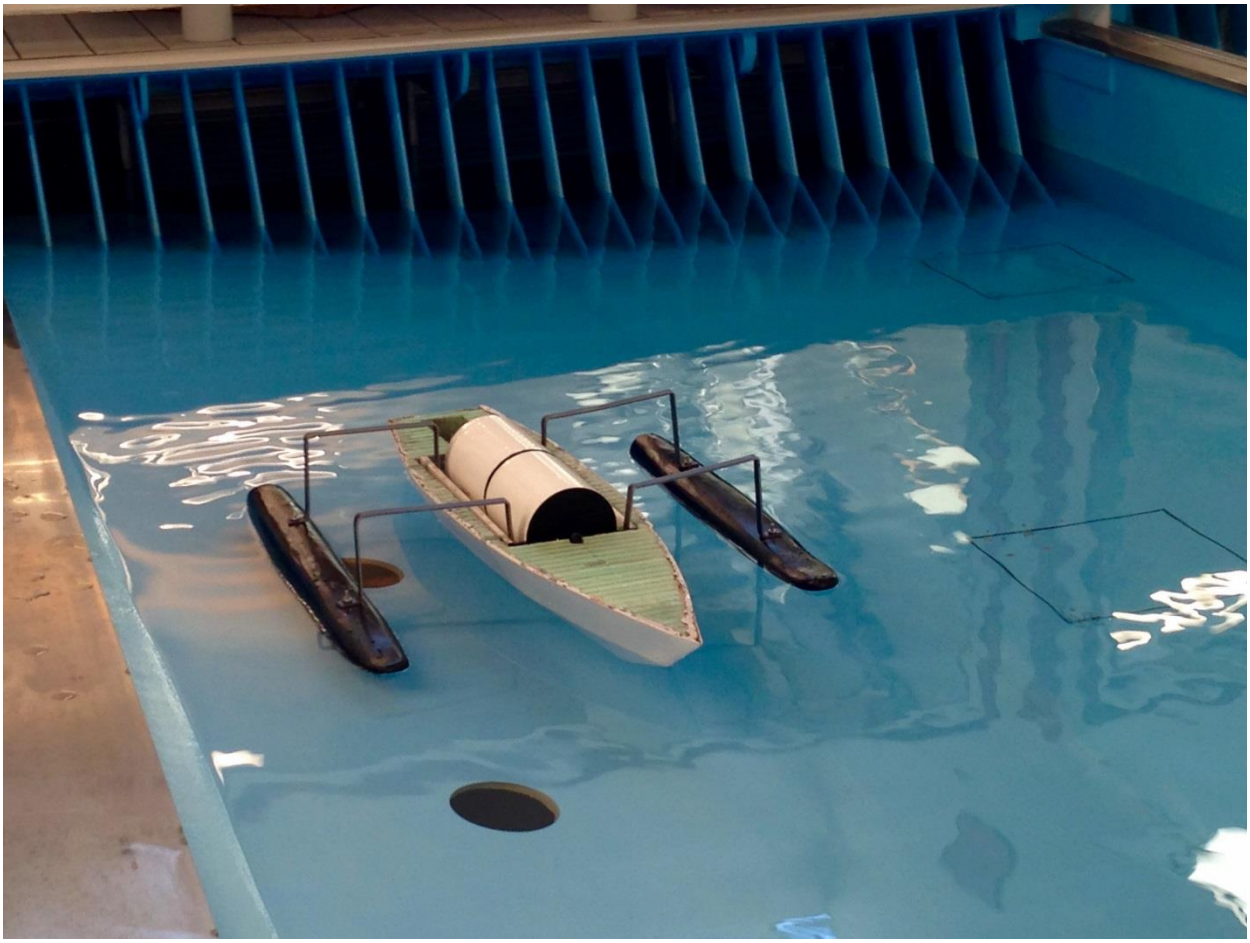

Figure 39: WAEV-1 Maiden Voyage in WPI Crew Tank.

After the vessel was situated properly in the water, the control cart was powered on, with the autotransformer set to 0V. The voltage was slowly increased until an arc was struck in the spark gap, which was 7.98kV. The ensuing water-arc explosion was subjectively quite large, and some minimal motion was noticeable, even after the first explosion. After firing the first arc, it was

noticed that subsequent arcs were not firing properly. While the capacitor was discharging periodically, the voltage only increased to around one or two kilovolts, which was not high enough to trigger a water-arc explosion. The usual muffled bang audible during successful water-arc was not heard when the capacitor discharged, but rather a soft click was heard as stored energy was released.

After the capacitors were discharged to ensure safety, the WAEV-I was removed from the water for inspection. It was immediately obvious that there was significant bilge water in the hull, and the thruster components, including the spark gap, were wet. The moisture on the spark gap was theorized to lower the ionization potential of the gap, causing the capacitors to discharge prematurely. The source of the bilge water was thought to be from leakage due to poor seals in the thruster assembly, which were exacerbated by the pressure of the water-explosions. As such, the WAEV-I was able to fire a few initial explosions before the spark gap became wet.

In addition to leakage from the thruster assembly, when the vessel was lifted from the water, the bilge water was seen to leak from the hull itself. This indicated that the fiberglass covering on the hull contained voids, which allowed water to leak during operation.

Upon inspection of the GoPro footage, the source of the thruster assembly leakage was seen to be the spark gap threaded rod. To verify this, the thruster assembly was removed from the hull, and the chamber was filled with water. When 80PSI air pressure was applied to the chamber opening, water was seen to leak from the threaded hole, confirming the source of leakage. The image below in Figure 40 shows a frame from the GoPro footage, with the water being ejected from the thruster assembly.

Figure 40: Frame from GoPro onboard video with water splashes from chamber leaks.

6.9 Design Revisions and Vessel Modifications

Two shortcomings were exposed during the initial testing of the WAEV-I, hull leakage, and poor thruster seals. The former was solved by stripping the WAEV-I of its paint, applying two additional layers of fiberglass, and coating with several layers of marine Gel-Coat. To prevent leakage in the thruster assembly, the assembly underwent significant redesign, and the spark gap system was augmented to ensure continuous operation.

6.9.1 Hull modifications

The existing paint on the WAEV-I was removed by scraping with acetone as a solvent. The surface was then sanded until smooth before additional fiberglass was added. The woven fiberglass cloth used previously was thought to limit the saturation of resin. While the cloth does provide higher strength, a Chopped Strand Mat type fiberglass allows for higher resin penetration, and can be stretched to conform to contours more easily. As waterproofing is more important to the function of the WAEV-I, Chopped Strand Mat was chosen for the fiberglass application process. The mat was applied as before, with polyester resin. Small strips of mat were used instead of large sheets, in order to ensure proper adhesion in all areas.

Following the application of fiberglass mat, the WAEV-I was coated with several layers of clear un-waxed marine Gel-Coat. The Gel-Coat serves the purpose of filling any small voids in the fiberglass. Each coat provides a 20mil-thick layer of gel, and four coats were applied for a total

thickness of 80mil. After the un-waxed gel coat was allowed to cure to a tacky surface, a 20mil coat of white waxed Gel-Coat was applied to finish the hull. The WAEV-I after application of Gel-Coat can be seen in Figure 41 below.

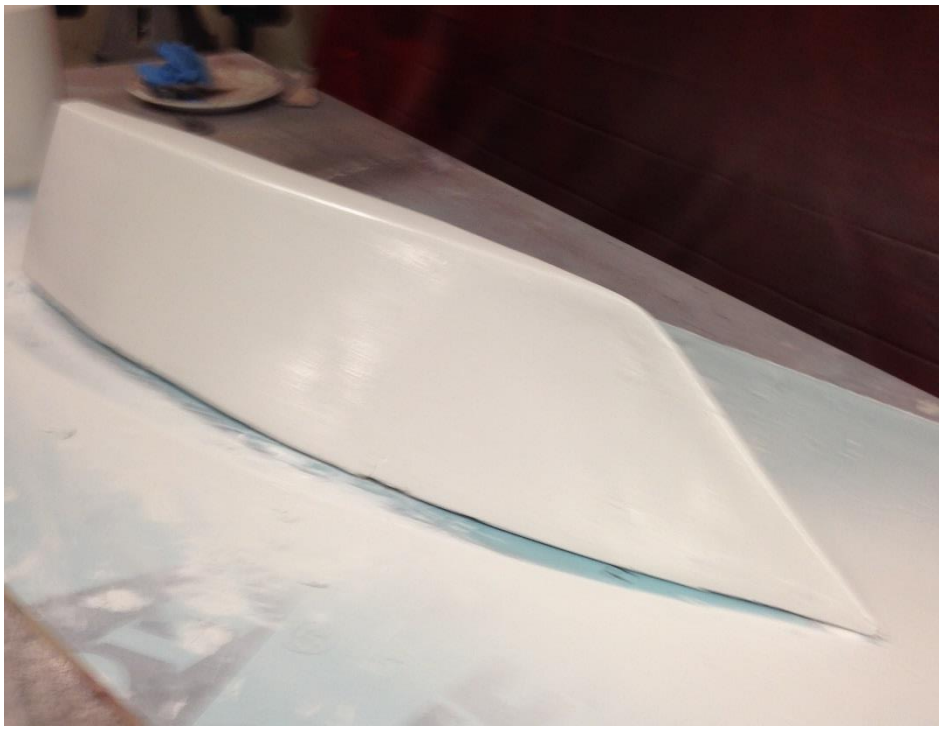

Figure 41: Vaka hull after application of Gel-Coat.

The resulting coat was very hard and durable, and was waxed with automotive wax to impart a high luster. The vaka was reassembled by installing the thruster and capacitors as before, and then mounting the ama's. Aluminum brackets were machined and installed into the vaka hull with rivets, in order to mount the acrylic covering, instead of construction adhesive. This was done in order to allow the cover to be easily removed for modifications. An image of the WAEV-I after final assembly is shown in Figure 42 below.

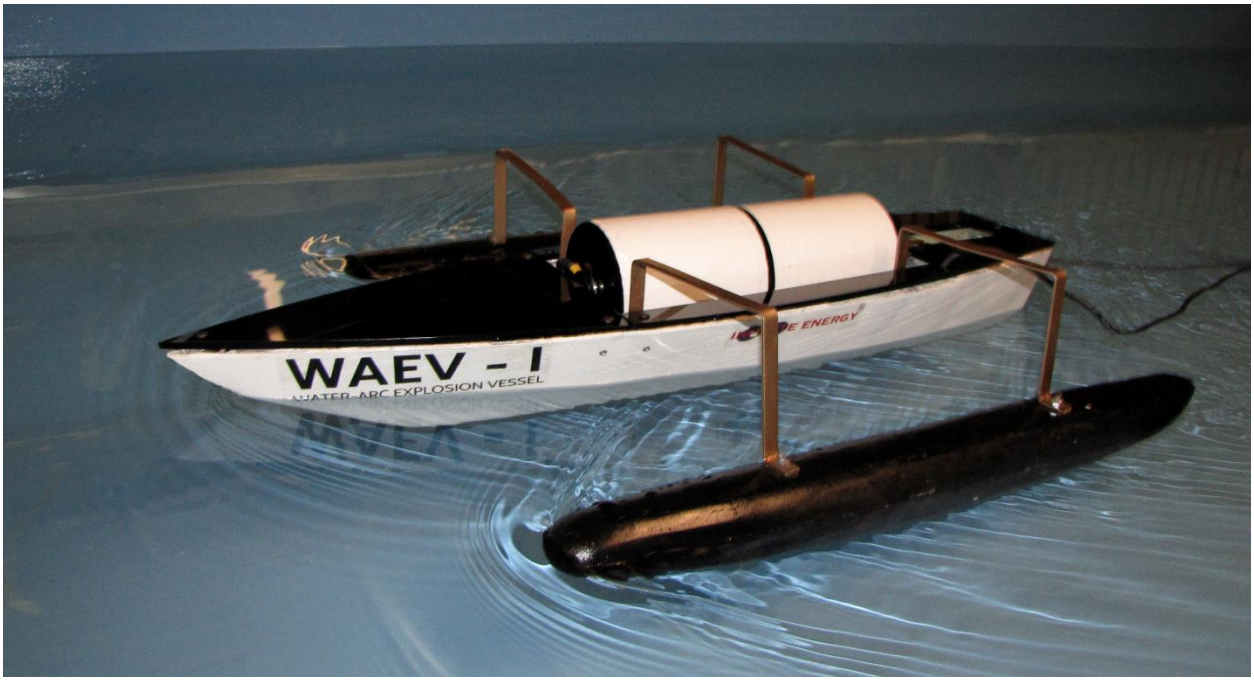

Figure 42: Final assembly of WAEV-I in water

6.9.2 Thruster Design Revisions

Analysis of the footage of the spark gap system obtained from the GoPro, as well as a verification test conducted with air pressure suggested that leakage from the thruster assembly was causing the spark gap to become wet. To prevent the thruster from leaking, a significant redesign of the assembly was completed.

The stainless steel chamber was replaced with an aluminum one, for easier machinability and thus tighter tolerances. The chamber was also threaded on a CNC lathe rather than being cut by hand with a die, which allowed for 1”-8 threads between the chamber and the UHMW block. The large pitch of these threads reduced the stress on the UHMW when tightening, allowing for a much tighter seal. To further increase the performance of the seals under the high pressures generated during explosions, a high-density 4mil thick Teflon tape was applied to the threads prior to insulation, and a nitrile O-ring was placed at the end of the chamber. As before, any wet-dry interfaces were waterproofed with silicone caulking.

In addition to increasing the performance of the thruster’s seals, the integrated adjustable spark gap housed within the thruster assembly was also modified, to increase its simplicity and number of components. This resulted in a much more reliable spark gap switch, and also allowed for easier adjustment. While the original design made use of a threaded rod and cap nut in order to

provide an electrical connection to the explosion chamber, the redesigned spark gap omitted these components by using the OD of the explosion chamber itself as a spark gap electrode. The opposing spark gap electrode was comprised of a thumb screw and stainless steel cap nut. These were threaded into a steel extension arm connected to the capacitor mounting rod. A rendering of the redesigned thruster assembly is shown in Figure 43.

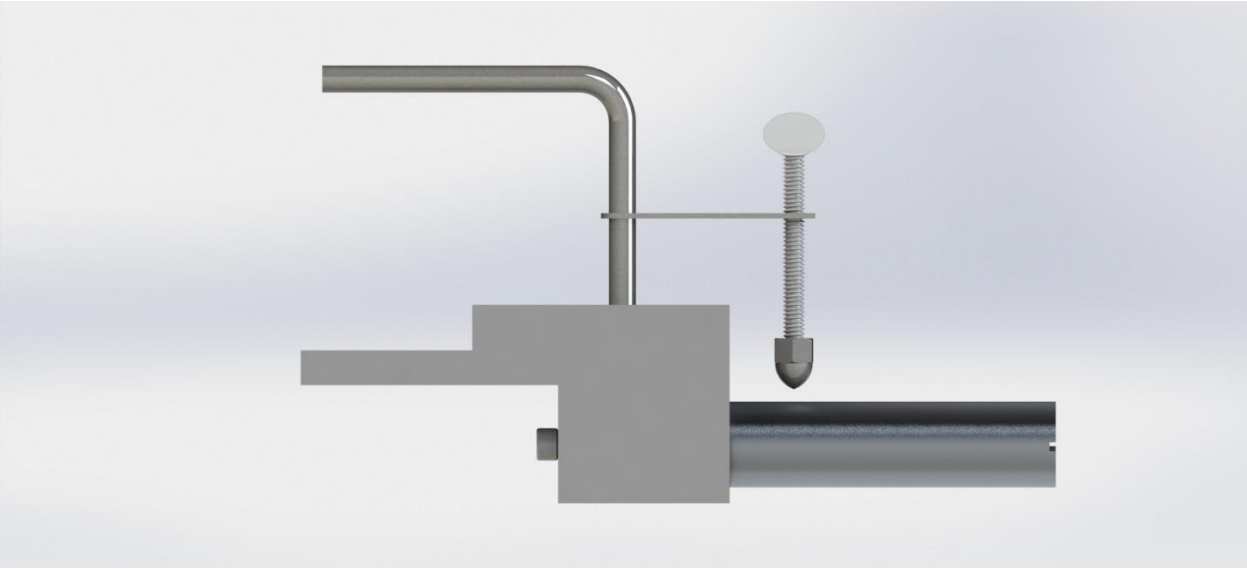

Figure 43: Rendering of final thruster assembly

The redesigned thruster contained fewer components and was thus far simpler than the original. These design constraints were selected to ensure reliable operation under the high stresses imposed by water-arc explosions, and to reduce the possibility of water leakage impairing the function of the spark gap. Testing was conducted to ensure these goals were met, which is described in the following section.

6.10 Final Testing and Results

To provide as much data as possible, much more sophisticated testing procedures were developed during the final testing of the WAEV-I compared to previous testing. The WAEV-I was closely filmed in high-resolution during all testing, to allow for analysis of velocity and pulse timing, as well as to provide a means for close subjective observation.

6.10.1 Experimental Design

In addition to the camera, a cable was threaded through the WAEV-I's akas, and stretched along the direction of travel. The cable was marked at the starting location, as well as at a point 6 meters away from it. The video footage showed the WAEV-I travel between these two points, and provided a time of travel, from which velocity was calculated.

As it was repeatedly demonstrated that water-arc explosion produce a rapid impulse rather than a sustained force, it was desired to determine the magnitude of the impulse. To achieve this goal, a MEMS accelerometer system was implemented onboard the WAEV-I. The system was comprised of an Invensense MPU6050 Inertial Measurement Unit (IMU), a lithium-ion battery, a boost converter, an SD card storage system, and an Arduino Uno Microcontroller. These components were placed inside a sealed plastic container, and affixed to the WAEV-I's hull.

The single cell Li-ion battery pack provides 3.7V nominally, which is below the Arduino's operating voltage of 5V. The boost converter module steps the 3.7V up to provide the Arduino with 5V. The SD card is inserted into a breakout board, and connected to the Arduino over a Serial Peripheral Interface (SPI) bus. The Arduino also communicates over I^2C to obtain accelerometer conversions from the MPU6050 IMU, and logs these to the SD card for later processing on a PC in Matlab. The Arduino is prompted to begin data collection by grounding a digital input pin, which is achieved by inserting a jumper wire, modeled above as an SPST switch.

6.10.2 Results

The WAEV-I was placed in the water, and the power supply was turned on. The WAEV-I was allowed to travel the 6 meter distance between the marked positions on the cable before the power supply was switched off and the capacitors were discharged. The spark gap was adjusted to fire at 7.97kV, and the capacitors discharge at a rate of once in 1.6 seconds, or 0.63Hz. Following several such 6 meter trials, data processing was completed, including velocity calculations, accelerometer processing, and video analysis.

The WAEV-I took an average of 33 seconds to travel the 600 centimeter span between the marked points on the cable. This results in a velocity of $\frac{600cm}{33s} = 18cm/s$. While this velocity is fairly low, the achievement of consistent motion was a demonstration of functional success of the WAEV-I's water-arc propulsion system.

While the velocity measurements provided useful results for the motion of the vessel, processing the accelerometer data obtained from the SD card yielded inconclusive results. The Arduino was able to write several lines of data to the SD card, however when plotted in Matlab, the data showed several very high peaks, as well as periods of flat-lines, apparently at zero g. This was inconsistent with the expected acceleration data, since the maximum acceleration force of the MPU6050, indicated by the high peaks on the plot, was very unlikely to be reached by the WAEV-I. Additionally, the flat-lines at zero g are also very unlikely, since the small fluctuations in velocity would cause nonzero acceleration, even between explosions.

Prior attempts at integrating control electronics into a water-arc explosion system showed that the electromagnetic (EM) interference due to the high voltage wiring caused stray voltages to be induced in the control electronics, resulting in sporatic behavior. As this occurrence was previously observed, it was likely that EM was also the cause of the apparent corruption of the accelerometer data. The peaks in the plot are likely due to high voltages induced in the wiring, and the periods of zero g reading could be explained by the induced voltages triggering the protection circuitry contained within the MPU6050. It is notable that the peaks indicate a value of ±32767, which is the maximum value that can be stored in an integer datatype on the Arduino's 16-bit architecture.

Though the accelerometer data was inconclusive, the final testing of the WAEV-I yielded several quantitative indicators of the performance of the WAEV-I. The WAEV-I was also evaluated by measuring the final mass to be 9.5kg, indicating an average thrust force of 10N. This is consistent with thrust force measurements conducted on previous explosion chambers. During testing, it was noticed that the tether cables imposed a significant elastic force on the vessel, opposing the thrust force of the propulsion system. Integration of an onboard power supply would have eliminated this force, likely demonstrating higher performance.

7. Conclusions and Recommendations

From the extensive testing of water arc explosions and through the construction of the WAEV-1 vessel, the team was able to devise the following conclusions and recommendations for the progression of this new, innovative technology. The prior art discussed in this paper and the experimental results has also given the team insight on future experiments that could be conducted to advance water arc propulsion technology. In this chapter, the team has presented their conclusions on the performance and capabilities of the WAEV-1 vessel as well as the feasibility of water arc propulsion technology as a whole.

7.1 The WAEV-1

The WAEV-I demonstrates groundbreaking progress in marine propulsion as a new and innovative, solid-state, alternative energy technology. By successfully constructing a craft capable of harnessing the power of electrodynamic water-arc propulsion, the potential for future water-arc propelled crafts can be visualized. One of the clear benefits of this new propulsion technology being applied to marine crafts is that it greatly reduces the number of transduction stages needed to provide propulsion. For example, in an electric boat, the electricity stored in batteries would run through an electric motor to provide mechanical rotation. This mechanical energy would then rotate a propeller, moving the surrounding, water forcing the boat forward. In this application there are at least two transduction stages before the stored energy can provide motion for the boat. This presents the opportunity for energy losses at each stage, ultimately lowering the total efficiency of the device. With the water-arc propulsion system implemented in the WAEV-1, there is only one transduction stage and it is solid-state. This not only reduces the amount of potential energy losses by having less trandsduction stages but also reduces the energy lost to forces such as the friction of a propeller in the water.

While the efficiency of the WAEV-1 is currently low, water-arc propulsion technology exhibits the potential for rapid performance increases with additional development. Battery technology is also a growing field which could provide the means for the WAEV-1 to operate independent from a tether. Advancements in high voltage power supplies could reduce the weight of the vessel, allowing the WAEV-1 to reach high speeds and accelerations making it more versatile. With these improvements, the WAEV-1 could prove to be a groundbreaking model for higher efficiency, solid-state, small, unmanned crafts.

7.2 Electrodynamic Water-Arc Propulsion Feasibility

Before the team began experimenting with electrodynamic water-arc propulsion, it had only been tested in open air laboratory environments. Over the past 8 months, the team has been able to take this technology and apply it in an underwater setting, proving that water-arc explosions still produce significant thrust while submerged. This lends itself to being used in aquatic crafts such as the WAEV-1.

As mentioned before, the efficiency of the current water-arc explosion thruster is somewhat low. However, even with its low efficiency, the WAEV-1 was still capable of moving solely off the power of the water-arc thruster. This demonstrates a clear potential for electrodynamic water-arc propulsion. If motion can be achieved with a low efficiency thruster, as the technology becomes more developed in the future, the ability to move either larger crafts or increase the speed of smaller vessels will be proportional to advances in the efficiency.

Currently, the water-arc thruster is used as a pulse jet in which a water explosion occurs every 1.6 seconds. While the firing rate could be increased to improve the thrust output of the system, the team believes that there are other, more fruitful ways of improving this technology. Pulse jet setups can lend themselves to different applications where a fuel is burned in pulses. However, in many of these uses, the energy to activate an explosion is relatively low. In order to trigger a water-arc explosion, a high energy arc must be created through the water in the chamber. The amount of energy needed to turn the surrounding environment into a plasma so an arc can be created requires a very high electric potential as well a significant amount of energy. Since in a water-arc thruster an arc has to be created for every pulse, a large portion of the stored energy is used to generate an arc, rather than thrust. The team believes that this could be a major cause for why the efficiency is currently low.

To solve this problem, both the team and Graneau have theorized a continuous water explosion jet with a constant arc. When creating an arc, as mentioned above, a large portion of the energy goes into creating the plasma in the surrounding environment but once the plasma has been created, it provides a low impedance path for electricity to flow. This means that once an arc has been created, the voltage can be greatly reduced to a point where an arc is still sustained allowing energy to flow through the explosion chamber. During the sustained arc, the current will remain high allowing the chamber to also be used as an MHD thruster. As mentioned in the background

of MHD propulsion, the explosion chamber would be able to utilize Lorentz Force to propel water out of the chamber.

One of the challenges in creating this continuous jet is designing a power supply that can adapt to the energy needs of the explosion chamber. To initialize the explosion, the power supply will have to deliver a high energy pulse using capacitors similar to the ones used on the WAEV-1. Once an initial arc has been fired, the power supply has to continue to provide an uninterrupted steam of DC current with a voltage high enough to sustain the arc. Unlike, the power supply needed to charge the capacitors (high voltage, lower current), the power supply would have to adapt to allow a large amount of current to flow into the chamber. While this may be a challenging task, the team believes that it is feasible through additional development.

Once a continuous arc is generated, the design of the explosion chamber must also change to facilitate a continuous thrust. This chamber design would ultimately been similar to the team's third chamber revision where there was an inlet and an outlet for the chamber rather than a single outlet. By having two openings in the chamber, a steady stream of water would be able to be propelled through the explosion chamber generating a continuous thrust. As seen through the testing of the team's third chamber design, a challenge in designing this thruster would be to restrict the backwards flow of water through the inlet once an initial explosion has been fired. However, the team believes that through the utilization of electronically controlled valves, or solid-state valves such as a Telsa valve, a new jet design will be capable of creating a continuous stream of thrust.

The fact still remains that the exact causes of this phenomenon are unknown, and that any development into different methods of producing water arc explosions could reveal enough to devise even more efficient systems. For this reason, the team encourages additional experimentation to be conducted to advance solid-state technology to new heights. From developing the first successful, solid-state, water-arc propelled craft with the WAEV-1, the potential for water-arc explosions to become a high efficiency means of aquatic propulsion is truly in what lies ahead.

7.3 Impact and Implications

The development of a new, solid-state, aquatic propulsion is truly groundbreaking in the field of marine technology. With the development of a continuous, water-arc thruster, the feasibility of using this technology on a range of crafts will be greatly increased. This would lend the technology to be able to be used in a variety of applications where traditional propellers are unable to be used. An example of an application where propellers are not optimal is with underwater stealth operations in a submarine. This could inherently be useful for military operations but also scientific experiments such as providing minimal disturbance of aquatic life while observing them in their natural environment.

While this technology utilizes a high energy, electric pulse, the main source of thrust comes from the water itself. This means that by applying water-arc propulsion to aquatic crafts, the thruster would essentially be submerged in its own fuel. As the efficiency of water-arc thrusters increases, the ability to harness the energy within the water for thrust would also be increased, lowering the dependence on current energy generation. This alternative fuel technology is something that has not been greatly explored and could provide an additional source of green power in the future.

7.4 Future Work

With the successful implementation of an electrodynamic water-arc thruster to a marine craft comes the opportunity for improvement. As demonstrated in the previous sections, there is clear value in furthering advancements in this technology to create a higher efficiency solid-state propulsion system. This can mainly be accomplished through the design and construction of a continuous water-arc thruster. The construction of such a device would be a great advancement in water-arc technology, exposing the true potential of water-arc propulsion.

Future work into developing a variable high voltage power supply to facilitate a continuous jet would also further the advancement of water-arc propulsion. However, the output of the power supply isn’t the only aspect of its design that should be considered. Optimizing the design for weight could also play a large role in the success of water-arc propulsion. By avoiding large, iron transformer cores, the weight of the power supply could be greatly reduced allowing the entire power supply of the system to be placed on the craft rendering it completely wireless.

7. Conclusions and Recommendations

While creating a continuous water-arc thruster would be a significant advancement, additional research still needs to be conducted to gain a better understanding of the driving force behind water-arc explosions. The exact causes of the phenomenon are still debated and thus developing a greater understanding of the science behind this technology could lead to greater optimization in the design of a chamber and all of its subcomponents. With these advancements in the understanding and abilities of water-arc propulsion, a higher-efficiency, solid-state propulsion system may be able to facilitate the implementation of a new green, alternative energy as well as an innovative method of providing thrust for small-scale marine vessels.

8. Appendix

N.B. A digital appendix is supplied separately, as an addendum to this section.

8.1 2CL77 High Voltage Diodes

2CL69 through 2CL77

HIGH VOLTAGE, LOW CURRENT
SILICON RECTIFIER DIODES

EDI TYPE #	2CL69	2CL70	2CL71	2CL72	2CL73	2CL74	2CL75	2CL76	2CL77
PRV VOLTS	4,000	6,000	8,000	10,000	12,000	14,000	16,000	18,000	20,000
Forward Voltage Drop at 25°C & 10mA	20.0V	23.0V	25.0V	30.0V	37.5V	42.5V	50.0V	55.0V	62.5V
Cathode Mark	▲V▲	◀◀◀	<<<	◆◆◆	◆◆◆	●●●	●●●	∿∿∿	∿∿∿

ELECTRICAL CHARACTERISTIC
(at T_{Air} = 25°C Unless Otherwise Specified)

2CL FAST RECOVERY

Average Maximum Forward Current I_F Max @ T_{Air} = 30°C	5.0 mA
Max Surge Current (1 Cycle)	0.5 A
Max DC Reverse Current (25°C)	2.0 µA
Max DC Reverse Current (100°C)	5.0 µA
Reverse Recovery Time	100 nano Sec.
Max Virtual Junction Capacitance, C_j @ V_r = 0 (f=1Mhz.)	1.0 pico farads

NOTES: It is recommended that a proper heat sink be used on the terminals of this device between the body and the soldering point to prevent damage from excess heat.

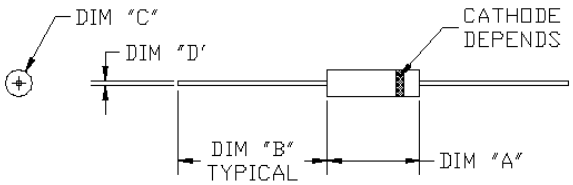

TYPE #	DIM "A"	DIM "B"	DIM "C"	DIM "D"
2CL69-71	0.31 IN (8.0 mm)	1.02 IN (26.0 mm)	0.12 IN (3.0 mm)	0.024 IN (0.6 mm)
2CL72-74	0.39 IN (10.0 mm)			
2CL75-77	0.47 IN (20.0 mm)			

EDI reserves the right to change these specifications at any time without notice.

ELECTRONIC DEVICES, INC. DESIGNERS AND MANUFACTURERS OF SOLID STATE DEVICES SINCE 1951.
21 GRAY OAKS AVENUE * YONKERS. NEW YORK 10710 914-965-4400 * FAX 914-965-5531 * 1-800-678-0828
e-mail:sales@edidiodes.com * website: http://www.edidiodes.com

8. Appendix

8.2 BK Precision High Voltage Probes – PR28A

SPECIFICATIONS

Voltage Range DC:	1 kV to 40 kV
Voltage Range AC:	1 kV to 28 kV rms
Divider Ratio	1000:1
Input Resistance:	1000 megohms, nominal
Accuracy DC:	±3%, plus meter accuracy
Accuracy AC:	±5%, plus meter accuracy @ 50/60 Hz
Dimension	16-1/2" x 2-1/8 x 2"
Cable Length	34"
Probe Tips	Two interchangeable screw-in types, one round needle and one special flat spring.
Safety	IEC1010, EN61010

BK PRECISION ®

4353 West Lawrence
Chicago, Illinois 60630

480-795-9-001 A

Printed in Taiwan

INSTRUCTION MANUAL

BK PRECISION ®

HIGH VOLTAGE PROBE
MODEL PR-28A

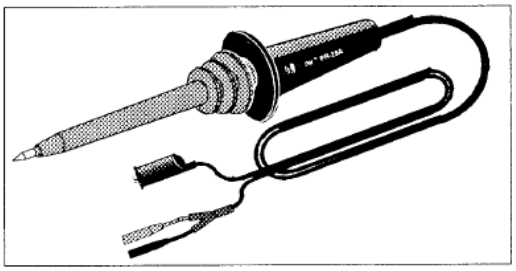

9.4 Gigavac G2SP High Voltage Relay

G2 **15 kV**

No Load Switching

RoHS Compliant, date code 0701 and later

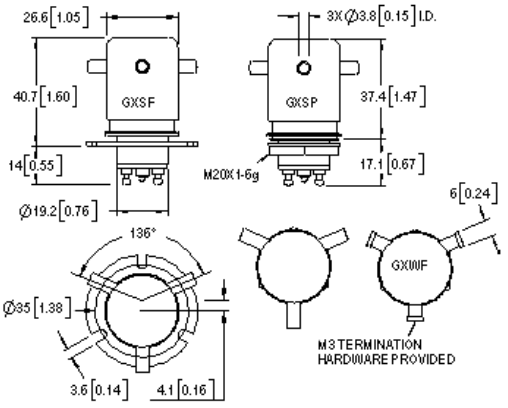

FEATURES

- High carry current, 50Adc continuous, in a small package
- Low, stable contact resistance minimizes loss in RF circuits
- Two mounting styles available, flange or through panel with jam nut
- Solder or threaded high voltage connections help make installation easy
- User interchangeable coils provide for driver versatility
- Meets or exceeds standards set in MIL-R-83725

PRODUCT SPECIFICATIONS

Contact & Relay Ratings	Units	G2
Contact Form		C
Contact Arrangement		SPDT
Voltage, Test Max., Contacts & to Base (15 µA Leakage Max., dc or 60Hz)	kV Peak	17
Voltage, Operating Max., Contacts & to Base (15 µA Leakage Max.)		
dc or 60 Hz	kV Peak	15
2.5 MHz	kV Peak	12
16 MHz	kV Peak	9
32 MHz	kV Peak	7
Current, Continuous Carry Max		
dc or 60 Hz	Amps	50
2.5 MHz	Amps	30
16 MHz	Amps	17
32 MHz	Amps	10
Coil Hi-Pot (V RMS, 60 Hz)	V	500
Capacitance		
Across Open Contacts	pF	0.5
Contacts to Ground	pF	1
Resistance, Contact Max @ 1A, 28 Vdc	ohms	0.012
Operate Time	ms	15
Release Time	ms	9
Life, Mechanical	cycles	1 million
Weight, Nominal	g (oz)	84 (3)
Vibration, Operating, Sine (55-500 Hz Peak)	G's	10
Shock, Operating, 1/2 Sine11ms (Peak)	G's	50
Temperature Ambient Operating	°C	-55 to +125

COIL RATINGS

Nominal, Volts dc	12	26.5	115
Pick-up, Volts dc, Max.	8	16	80
Drop-Out, Volts dc	.5 - 5	1 - 10	5 - 50
Coil Resistance (Ohms ±10%)	60	250	3500

Ratings listed are for 25°C, sea level conditions

For more information, refer to

Relay User Instructions

G2 S F - 12Vdc

- High Voltage/ Power Terminal Connections: S = Solder Pot, W = Screw
- Mounting: F = Flange, P = Through Panel
- Coil Voltage*: Blank = 26.5 Vdc, 12Vdc = 12 Vdc, 115Vdc = 115 Vdc

*Order the relay with the coil voltage in the part number as shown above. The coil voltage will appear on the coil plate near the coil terminals rather than in the P/N on the relay.

01/11/11

9.5 HVP5-HVP! High Voltage Diode

RECTRON
SEMICONDUCTOR
TECHNICAL SPECIFICATION

HVP5 THRU HVP16

HIGH VOLTAGE ASSEMBLIED RECTIFIER

VOLTAGE RANGE 5000 to 16000 Volts CURRENT 0.75 Amperes

FEATURES
* Low cost
* Low leakage
* Isolated case
* Surge overload rating - 50 amperes peak
* Mounting position: Any
* Low forward voltage drop

MECHANICAL DATA
* Epoxy: Device has UL flammability classification 94V-O

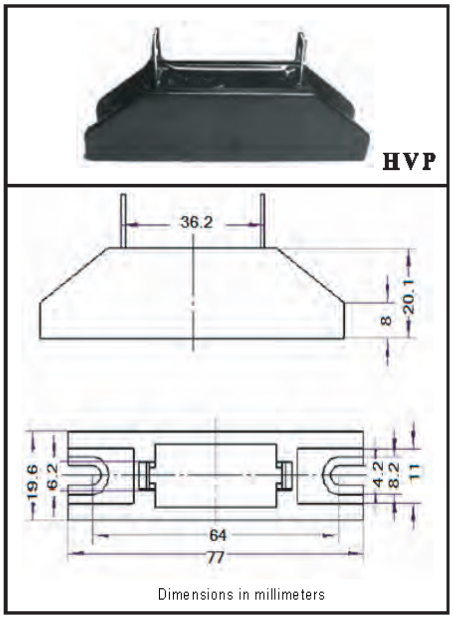

Dimensions in millimeters

MAXIMUM RATINGS AND ELECTRICAL CHARACTERISTICS
Ratings at 25 °C ambient temperature unless otherwise specified.
Single phase, half wave, 60 Hz, resistive or inductive load.
For capacitive load, derate current by 20%.

MAXIMUM RATINGS (At T_A = 25°C unless otherwise noted)

RATINGS	SYMBOL	HVP5	HVP8	HVP10	HVP12	HVP14	HVP15	HVP16	UNITS
Maximum Recurrent Peak Reverse Voltage	V_{RRM}	5	8	10	12	14	15	16	K Volts
Maximum RMS Voltage	V_{RMS}	3.5	5.6	7.0	8.4	9.8	10.5	11.2	K Volts
Maximum DC Blocking Voltage	V_{DC}	5	8	10	12	14	15	16	K Volts
Maximum Average Forward Rectified Current at T_A = 50°C	I_O	750							mAmps
Peak Forward Surge Current 8.3 ms single half sine-wave superimposed on rated load (JEDEC method)	I_{FSM}	50							Amps
Operating and Storage Temperature Range	T_J,T_{STG}	-55 to +150							°C

ELECTRICAL CHARACTERISTICS (At T_A = 25°C unless otherwise noted)

CHARACTERISTICS	SYMBOL	HVP5	HVP8	HVP10	HVP12	HVP14	HVP15	HVP16	UNITS
Maximum Instantaneous Forward Voltage at 0.75A DC	V_F	8.0	14.0						Volts
Maximum DC Reverse Current at Rated DC Blocking Voltage	I_R	5.0							uAmps

NOTES: Enough heat sink must be considered in application.

2013-01

RATING AND CHARACTERISTIC CURVES (HVP5 THRU HVP16)

FIG. 1 - TYPICAL FORWARD CURRENT DERATING CURVE

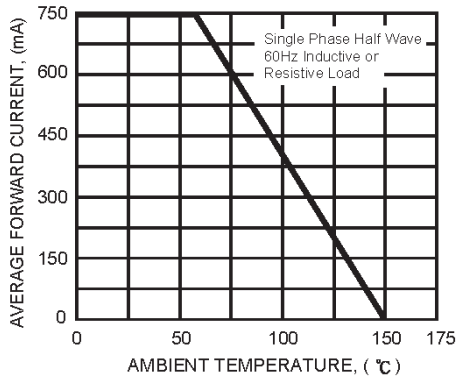

FIG. 2 - MAXIMUM NON-REPETITIVE FORWARD SURGE CURRENT

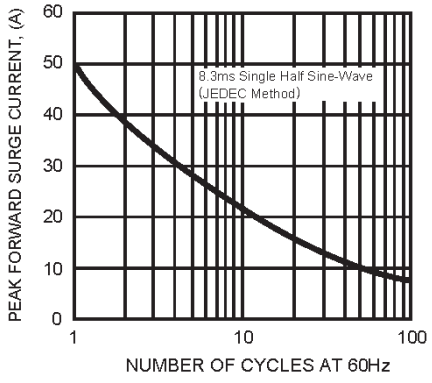

FIG. 3 - TYPICAL REVERSE CHARACTERISTICS

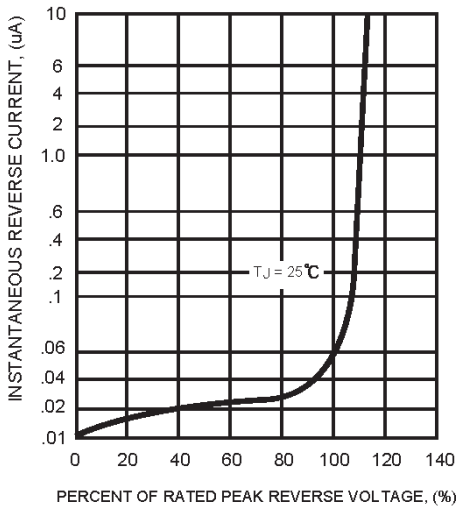

FIG. 4 - TYPICAL INSTANTANEOUS FORWARD CHARACTERISTICS

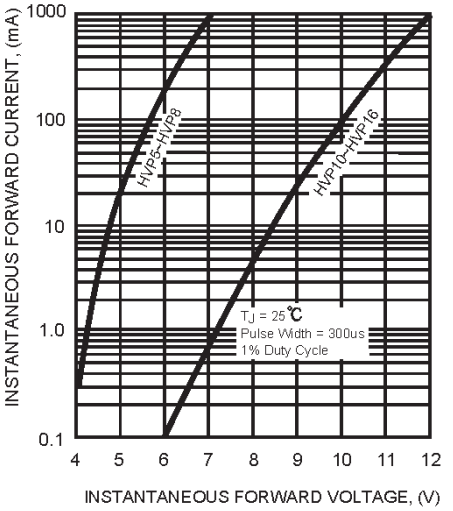

RECTRON

Attachment information about HVPXX

1. Marking on the body

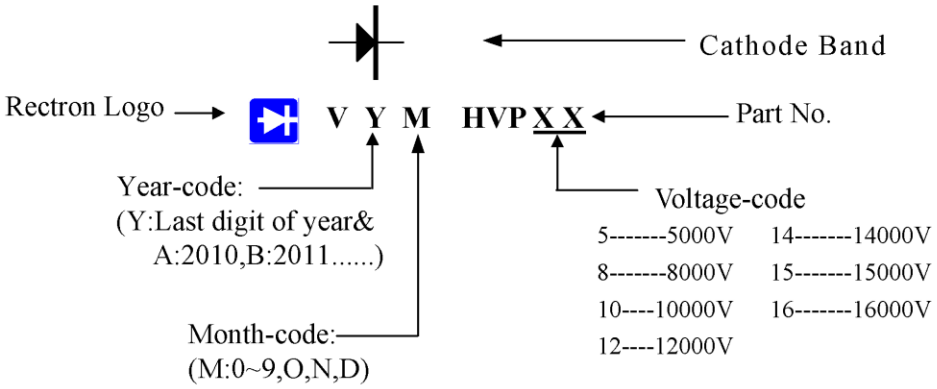

2. Items marked on the carton

CUSTOMER
TYPE
QUANTITY
LOT NO.
REMARK

DISCLAIMER NOTICE

Rectron Inc reserves the right to make changes without notice to any product specification herein, to make corrections, modifications, enhancements or other changes. Rectron Inc or anyone on its behalf assumes no responsibility or liability for any errors or inaccuracies. Data sheet specifications and its information contained are intended to provide a product description only. "Typical" parameters which may be included on RECTRON data sheets and/ or specifications can and do vary in different applications and actual performance may vary over time. Rectron Inc does not assume any liability arising out of the application or use of any product or circuit.

Rectron products are not designed, intended or authorized for use in medical, life-saving implant or other applications intended for life-sustaining or other related applications where a failure or malfunction of component or circuitry may directly or indirectly cause injury or threaten a life without expressed written approval of Rectron Inc. Customers using or selling Rectron components for use in such applications do so at their own risk and shall agree to fully indemnify Rectron Inc and its subsidiaries harmless against all claims, damages and expenditures.

8.3 UHMW Polyethylene

UHMW-PE
(ultra high molecular weight polyethylene)

POLYSTONE® M

Polyethylene is a low cost, chemically resistant plastic material that can be used for a wide variety of applications. The versatility of polyethylene has made it one of the world's most popular plastics. Polyethylene is available in a number of grades according to its molecular weight.

UHMW-PE (ultra high molecular weight polyethylene) is an extremely tough and abrasion resistant thermoplastic that is used for applications that require durability and/or abrasive wear resistance.

UHMW sheet is often used for lining chutes and hoppers in order to protect metal surfaces and promote the flow of solid materials such as sand, wood chips, or coal. UHMW is also used for packaging, conveyor, and food processing machinery parts including star wheels, idler sprockets, and under-chain wear strips.

RÖCHLING Engineered Plastics

KEY CHARACTERISTICS:

- Extremely tough and durable
- Low friction
- Excellent abrasion resistance
- Good chemical resistance
- Low water absorption
- Easy to fabricate
- Reprocessed grades available
- Enhanced bearing and wear grades available
- FDA compliant grades available

APPLICATIONS:

- Chute liners and hopper liners
- Wear strips
- Star wheels
- Idler sprockets
- Packaging machinery components
- Food processing machinery components

POLYETHYLENE TYPICAL PROPERTIES:

	UNITS	ASTM TEST	LDPE	HDPE	UHMW-PE
Tensile strength	psi	D-638	1,400	4,000	3,100
Flexural modulus	psi	D-790	30,000	200,000	110,000
Izod impact (notched)	ft-lbs/in of notch	D-256	no break	1.3	18.0*
Heat deflection temperature @66 psi	°F	D-648	122	172	-
Maximum continuous service temperature in air	°F		-	-	180
Water absorption (immersion 24 hours)	%	D-570	0.10	0.10	slight
Coefficient of linear thermal expansion	in/in/°F x 10^{-5}	D-696	-	7.0	11.1

UHMW Standard Sizes: SHEET: 48"x96" (0.062"-4.0" thick), 48"x120" (0.062"-7.0" thick), 48"x144" (0.375"-4.0" thick), 60"x96" (0.375"-4.0" thick), 60"x120" (0.375"-4.0" thick) POLYSTONE® MEGASHEET: 96"x240" (0.375"-4.0" thick) ROD: diameter 0.25"-10.00" TUBE: diameter 2.0"-9.398"

Length, width, thickness, and diameter tolerances vary by size and by manufacturer • Custom sizes and colors available upon request • Many of our materials are available as films with thicknesses of 0.029" or less. Values may vary according to brand name. Please ask your Curbell Plastics representative for more specific information about an individual brand. *Double-15° notch

Curbell Plastics has been supplying plastic sheet, rod, tube, films, adhesives, sealants, and prototyping materials for over 65 years

CURBELL PLASTICS
NATIONWIDE
1.888.CURBELL
www.curbellplastics.com

UHMWDataSheet 0308

8.4 1N4728A Zener Diode

Zener Diodes

FEATURES

- Silicon planar power Zener diodes
- For use in stabilizing and clipping circuits with high power rating
- Standard Zener voltage tolerance is ± 5 %
- AEC-Q101 qualified
- Material categorization: for definitions of compliance please see www.vishay.com/doc?99912

Pb e2 RoHS COMPLIANT HALOGEN FREE

APPLICATIONS

- Voltage stabilization

PRIMARY CHARACTERISTICS		
PARAMETER	VALUE	UNIT
V_Z range nom.	3.3 to 100	V
Test current I_{ZT}	2.5 to 76	mA
V_Z specification	Thermal equilibrium	
Int. construction	Single	

ORDERING INFORMATION			
DEVICE NAME	ORDERING CODE	TAPED UNITS PER REEL	MINIMUM ORDER QUANTITY
1N4728A to 1N4764A	1N4728A to 1N4764A -series-TR	5000 per 13" reel	25 000/box
1N4728A to 1N4764A	1N4728A to 1N4764A-series-TAP	5000 per ammopack (52 mm tape)	25 000/box

PACKAGE				
PACKAGE NAME	WEIGHT	MOLDING COMPOUND FLAMMABILITY RATING	MOISTURE SENSITIVITY LEVEL	SOLDERING CONDITIONS
DO-41	310 mg	UL 94 V-0	MSL level 1 (according J-STD-020)	260 °C/10 s at terminals

ABSOLUTE MAXIMUM RATINGS (T_{amb} = 25 °C, unless otherwise specified)				
PARAMETER	TEST CONDITION	SYMBOL	VALUE	UNIT
Power dissipation	Valid provided that leads at a distance of 4 mm from case are kept at ambient temperature	P_{tot}	1300	mW
Zener current		I_Z	P_V/V_Z	mA
Thermal resistance junction to ambient air	Valid provided that leads at a distance of 4 mm from case are kept at ambient temperature	R_{thJA}	110	K/W
Junction temperature		T_j	175	°C
Storage temperature range		T_{stg}	-65 to +175	°C
Forward voltage (max.)	I_F = 200 mA	V_F	1.2	V

ELECTRICAL CHARACTERISTICS (T_{amb} = 25 °C, unless otherwise specified)

PART NUMBER	ZENER VOLTAGE RANGE (1)	TEST CURRENT		REVERSE LEAKAGE CURRENT		DYNAMIC RESISTANCE f = 1 kHz		SURGE CURRENT (3)	REGULATOR CURRENT (2)
	V_Z at I_{ZT1}	I_{ZT1}	I_{ZT2}	I_R at V_R		Z_{ZT} at I_{ZT1}	Z_{ZK} at I_{ZT2}	I_R	I_{ZM}
	V	mA	mA	µA	V	Ω		mA	mA
	NOM.			MAX.		TYP.	MAX.		MAX.
1N4728A	3.3	76	1	100	1	10	400	1380	276
1N4729A	3.6	69	1	100	1	10	400	1260	252
1N4730A	3.9	64	1	50	1	9	400	1190	234
1N4731A	4.3	58	1	10	1	9	400	1070	217
1N4732A	4.7	53	1	10	1	8	500	970	193
1N4733A	5.1	49	1	10	1	7	550	890	178
1N4734A	5.6	45	1	10	2	5	600	810	162
1N4735A	6.2	41	1	10	3	2	700	730	146
1N4736A	6.8	37	1	10	4	3.5	700	660	133
1N4737A	7.5	34	0.5	10	5	4	700	605	121
1N4738A	8.2	31	0.5	10	6	4.5	700	550	110
1N4739A	9.1	28	0.5	10	7	5	700	500	100
1N4740A	10	25	0.25	10	7.6	7	700	454	91
1N4741A	11	23	0.25	5	8.4	8	700	414	83
1N4742A	12	21	0.25	5	9.1	9	700	380	76
1N4743A	13	19	0.25	5	9.9	10	700	344	69
1N4744A	15	17	0.25	5	11.4	14	700	304	61
1N4745A	16	15.5	0.25	5	12.2	16	700	285	57
1N4746A	18	14	0.25	5	13.7	20	750	250	50
1N4747A	20	12.5	0.25	5	15.2	22	750	225	45
1N4748A	22	11.5	0.25	5	16.7	23	750	205	41
1N4749A	24	10.5	0.25	5	18.2	25	750	190	38
1N4750A	27	9.5	0.25	5	20.6	35	750	170	34
1N4751A	30	8.5	0.25	5	22.8	40	1000	150	30
1N4752A	33	7.5	0.25	5	25.1	45	1000	135	27
1N4753A	36	7	0.25	5	27.4	50	1000	125	25
1N4754A	39	6.5	0.25	5	29.7	60	1000	115	23
1N4755A	43	6	0.25	5	32.7	70	1500	110	22
1N4756A	47	5.5	0.25	5	35.8	80	1500	95	19
1N4757A	51	5	0.25	5	38.8	95	1500	90	18
1N4758A	56	4.5	0.25	5	42.6	110	2000	80	16
1N4759A	62	4	0.25	5	47.1	125	2000	70	14
1N4760A	68	3.7	0.25	5	51.7	150	2000	65	13
1N4761A	75	3.3	0.25	5	56	175	2000	60	12
1N4762A	82	3	0.25	5	62.2	200	3000	55	11
1N4763A	91	2.8	0.25	5	69.2	250	3000	50	10
1N4764A	100	2.5	0.25	5	76	350	3000	45	9

Notes

(1) Based on DC measurement at thermal equilibrium while maintaining the lead temperature (T_L) at 30 °C + 1 °C, 9.5 mm (3/8") from the diode body

(2) Valid provided that electrodes at a distance of 4 mm from case are kept at ambient temperature

(3) t_p = 10 ms.

BASIC CHARACTERISTICS (T_{amb} = 25 °C, unless otherwise specified)

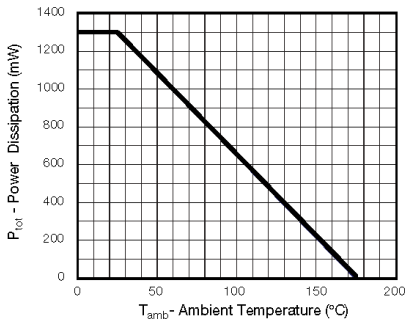

Fig. 1 - Admissible Power Dissipation vs. Ambient Temperature
$P_{tot} = f(T_{amb})$

PACKAGE DIMENSIONS in millimeters (inches): **DO-41_1N47xx**

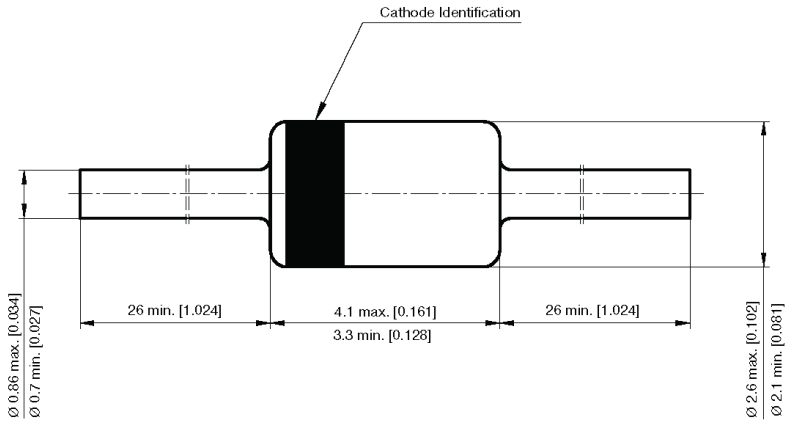

Document no. S8-V-3901.04-001(4)
Rev. 1 - Date: 30. Nov. 2011
22624

Disclaimer

ALL PRODUCT, PRODUCT SPECIFICATIONS AND DATA ARE SUBJECT TO CHANGE WITHOUT NOTICE TO IMPROVE RELIABILITY, FUNCTION OR DESIGN OR OTHERWISE.

Vishay Intertechnology, Inc., its affiliates, agents, and employees, and all persons acting on its or their behalf (collectively, "Vishay"), disclaim any and all liability for any errors, inaccuracies or incompleteness contained in any datasheet or in any other disclosure relating to any product.

Vishay makes no warranty, representation or guarantee regarding the suitability of the products for any particular purpose or the continuing production of any product. To the maximum extent permitted by applicable law, Vishay disclaims (i) any and all liability arising out of the application or use of any product, (ii) any and all liability, including without limitation special, consequential or incidental damages, and (iii) any and all implied warranties, including warranties of fitness for particular purpose, non-infringement and merchantability.

Statements regarding the suitability of products for certain types of applications are based on Vishay's knowledge of typical requirements that are often placed on Vishay products in generic applications. Such statements are not binding statements about the suitability of products for a particular application. It is the customer's responsibility to validate that a particular product with the properties described in the product specification is suitable for use in a particular application. Parameters provided in datasheets and/or specifications may vary in different applications and performance may vary over time. All operating parameters, including typical parameters, must be validated for each customer application by the customer's technical experts. Product specifications do not expand or otherwise modify Vishay's terms and conditions of purchase, including but not limited to the warranty expressed therein.

Except as expressly indicated in writing, Vishay products are not designed for use in medical, life-saving, or life-sustaining applications or for any other application in which the failure of the Vishay product could result in personal injury or death. Customers using or selling Vishay products not expressly indicated for use in such applications do so at their own risk. Please contact authorized Vishay personnel to obtain written terms and conditions regarding products designed for such applications.

No license, express or implied, by estoppel or otherwise, to any intellectual property rights is granted by this document or by any conduct of Vishay. Product names and markings noted herein may be trademarks of their respective owners.

Material Category Policy

Vishay Intertechnology, Inc. hereby certifies that all its products that are identified as RoHS-Compliant fulfill the definitions and restrictions defined under Directive 2011/65/EU of The European Parliament and of the Council of June 8, 2011 on the restriction of the use of certain hazardous substances in electrical and electronic equipment (EEE) - recast, unless otherwise specified as non-compliant.

Please note that some Vishay documentation may still make reference to RoHS Directive 2002/95/EC. We confirm that all the products identified as being compliant to Directive 2002/95/EC conform to Directive 2011/65/EU.

Vishay Intertechnology, Inc. hereby certifies that all its products that are identified as Halogen-Free follow Halogen-Free requirements as per JEDEC JS709A standards. Please note that some Vishay documentation may still make reference to the IEC 61249-2-21 definition. We confirm that all the products identified as being compliant to IEC 61249-2-21 conform to JEDEC JS709A standards.

9. References

[i] Ueyama, Yoshihiro, et. al. "Operation of the Thruster for Superconducting Electromagnetohydrodynamic Propulsion Ship 'YAMATO 1'" *Bulletin of the M. E. S. J.* Vol. 23 No.1 (March 1995): *Mitsubishi Heavy Industries, Ltd.*
[ii] http://www.kjmagnetics.com/
[iii] Standard Temperature and Pressure for Hydrogen Gas (273.15K, 1atm) - http://www.engineeringtoolbox.com/gas-density-d_158.html
[iv] Standard Temperature and Pressure for Oxygen Gas (273.15K, 1atm) - http://www.engineeringtoolbox.com/gas-density-d_158.html
[v] [v]Graneau, Peter, "Electrodynamic seawater jet: an alternative to the propeller?," *Magnetics, IEEE Transactions on* , vol.25, no.5, pp.3275,3277, Sep 1989 doi: 10.1109/20.42276
[vi] Johnson, Gary L., PhD. "Electrically Induced Explosions in Water. "Intersociety Energy Conversion Engineering (1992): 335-38.